

Theory of Coherent Van der Waals Matter

Igor M. Kulić^{1*} and Miodrag L. Kulić^{2†}

¹ *CNRS, Institute Charles Sadron, 23 rue du Loess BP 84047, 67034 Strasbourg, France and*

² *Institute for Theoretical Physics, Goethe-University D-60438 Frankfurt am Main, Germany*

(Dated: September 27, 2018)

We explain in depth the previously proposed theory of the coherent Van der Waals (cVdW) interaction - the counterpart of Van der Waals (VdW) force - emerging in spatially coherently fluctuating electromagnetic fields. We show that cVdW driven matter is dominated by many body interactions, which are significantly stronger than those found in standard Van der Waals (VdW) systems. Remarkably, the leading 2- and 3-body interactions are of the same order with respect to the distance ($\propto R^{-6}$), in contrast to the usually weak VdW 3-body effects ($\propto R^{-9}$). From a microscopic theory we show that the anisotropic cVdW many body interactions drive the formation of low-dimensional structures such as chains, membranes and vesicles with very unusual, non-local properties. In particular, cVdW chains display a logarithmically growing stiffness with the chain length, while cVdW membranes have a bending modulus growing linearly with their size. We argue that the cVdW anisotropic many body forces cause local cohesion but also a negative effective "surface tension". We conclude by deriving the equation of state for cVdW materials and propose new experiments to test the theory, in particular the unusual 3-body nature of cVdW.

PACS numbers: 82.70.Dd, 81.16.Dn, 82.70.Rr

I. INTRODUCTION

The major goal of physics is the quest for understanding and controlling the forces of Nature. In recent decades physicists and chemists have begun to invent increasingly creative ways to combine the fundamental forces and to generate new, effective interactions on microscopic and macroscopic scales. Cold atoms could not be trapped and cooled [1], colloidal suspensions would become unstable and flocculate [2], and magnetic levitation would be impossible [3] if combined, effective interactions were absent. As we know from condensed matter physics, the interplay of attractive and repulsive forces of different origins can give rise to highly complex structures. They range from gyroid phases in block copolymers [4], labyrinthine phases in ferrofluids [5] to nuclear pasta phases in neutron stars [6] to name only a few. Not surprisingly, adding more physical interactions naturally increases the structural complexity of the resulting materials. Here we ask the opposite question: how much complexity can emerge from a *single*, simple to generate, effective interaction?

In the recent short paper [7] we studied, the probably simplest *effective interaction* able to generate surprisingly complex structures. This effective interaction appears, for instance, between dipolar magnetic (or dielectric) particles when a spatially uniform, isotropic but time varying magnetic (or electric) field is externally applied (cf. Fig.1b). The first instance of it was described in a series of important papers by Martin et al. [8, 9] in a system of superparamagnetic colloids in *balanced triaxial*

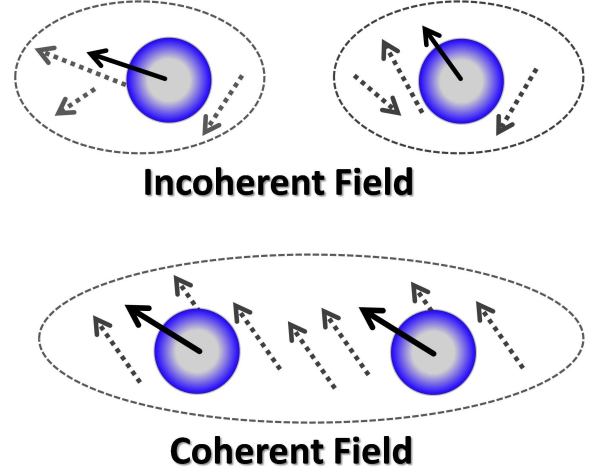


FIG. 1: (Top) The incoherent (Van der Waals-like) interaction VdW and (Bottom) spatially coherent fluctuation interaction cVdW are both induced by field fluctuations - but with different spatial correlations.

magnetic fields (BTMF) - rotating magnetic fields spinning on a cone with the magic opening angle $\theta_m \approx 54, 7^\circ$. The emerging effective interaction between two colloids appeared to be, at the first glance, reminiscent of the London-Van der Waals force [8–10]. Yet the structures formed, including colloidal membranes and foams, were unexpectedly more intricate and differing strongly from those expected in classical Van der Waals (VdW) systems.

Inspired by the fascinating magnetic colloid superstructures generated experimentally [8, 9, 11] we have begun to systematically investigate the physical ingredi-

*Electronic address: kulic@unistra.fr

†Electronic address: kulic@th.physik.uni-frankfurt.de

ents and the consequences of the induced interaction [7]. By starting out from the analogy with the VdW interaction we have considered a generalization of Martin's BTMF field structure [8, 9] and arrived at the concept of the *spatially coherent Van der Waals* (cVdW) interaction, see Fig.1b [12].

In the previous short and rather dense paper [7], we have answered the important question, why cVdW generates complex structures like chains, membranes and foams while its sister - the Van der Waals-like *incoherent fluctuation interaction* (VdW) – see Fig.1a, merely forms phase-separated lumps or 3D droplets of matter within a two phase system [13]. However, many details and numerous subtle questions were omitted in [7] due to the lack of space. In the following we close the gap and present a fairly complete theory of cVdW.

As a new item going much beyond the previous Letter [7], we study the bulk and finite size effects in chains, rings, membranes, spherical and cylindrical shells. In particular, we investigate the bending elasticity of chains and membranes and show that there is a qualitative difference with systems with short-range forces. As we will see, most structures formed by cVdW, have properties which are inherently dictated by *long range anisotropic many body forces*. They exhibit collective (i.e. scale and shape dependent) stiffness, surface tension and line tension.

The physical content of the paper is schematically represented in the Diagram in Fig.2, where the free-energy as a function of the *effective non-local susceptibility* $\hat{\chi}_{eff,ij}$ plays the central role in all our studies of cVdW systems. In the microscopic theory the latter contains the 3-body (and higher order) interactions, while in the macroscopic theory it can be expressed via an *effective demagnetization tensor* \hat{L} . Both approaches give rise to the *collective, long range, shape-sensitive* nature of the cVdW interaction.

The text is organized as follows. In *Section II* we briefly introduce the reader into the basic properties of the magnetorheological (MR) colloids and describe the first experimental realization of the cVdW interaction in such systems by Martin et al[8, 9]. In *Section III* we develop the basic physical and mathematical machinery to treat the cVdW interaction. We then derive the first central result of this paper: The time-averaged free-energy as the trace of the *effective non-local susceptibility tensor* $\hat{\chi}_{eff}$. The latter tensor describes an effective interaction between two colloids mediated by all the other colloids - thus containing all many body interactions. Based on the microscopic theory for the free-energy in *Section IV* we discuss cVdW systems and self-assemblies of colloids in various structures.

In *Section V* we study the formation of chains and membranes within the framework of a macroscopic mean-field theory. The consistency of the latter with the microscopic approach is discussed there as well. There we also show that the cVdW systems can be considered as systems with an effective *negative* surface energy. In *Section*

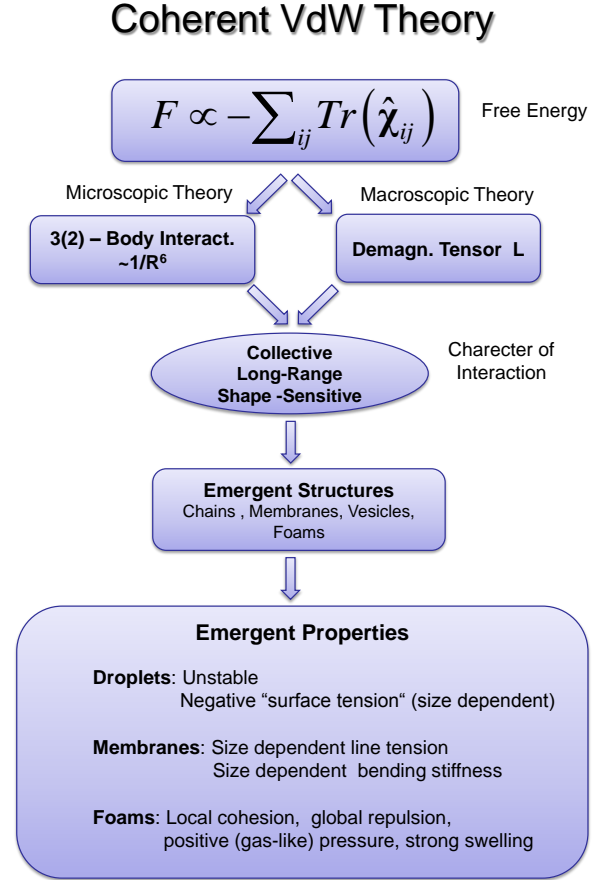


FIG. 2: Theory of the cVdW interaction: Outline of results derived in this paper.

VI we generalize the cVdW interaction to anisotropic objects and study the interaction between multiple elementary structures, including the bead-membrane and the two membrane interaction. The interaction turns out to be very rich, anisotropic and changes sign depending on the mutual orientation of the interacting objects. Based on these preparatory results, in *Section VII* we study the formation of the more complex emergent structures: the colloidal foams. We show that the cVdW theory predicts a positive pressure of the foam and that it swells against the gravitational field to notable heights.

The most notable quantitative results are summarized in two tables at the end of *Section X*. We conclude by pointing out interesting experimental effects and tests of the theory and by outlining some important open questions concerning cVdW. More detailed derivations of some formulas are contained in several Appendices for the interested reader. The mathematically less interested reader is invited to browse through the figures, each of which explains a new concept, and to run through them towards the Discussion.

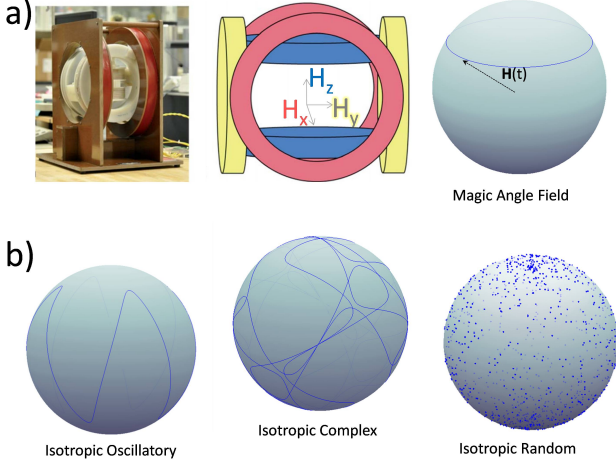


FIG. 3: a) The first realization of the cVdW interaction with triaxial magnetic fields by Martin et al. The field rotates on a cone with the "magic angle" (cf. text). To avoid torques the field rotation is inverted every cycle. b) Other possible realizations of the square-isotropic triaxial field. If induced torques are negligible (no net rotation on average), all isotropic excitations are equivalent and give rise to the same cVdW interaction.

II. PRELIMINARIES - MAGNETIC COLLOIDS IN BALANCED TRIAXIAL FIELDS

The study of responsive "smart materials" with remarkable properties has been intensifying in the last decades. In that respect the magnetorheological (MR) suspensions, made of magnetizable solid microparticles (colloids), dispersed in nonmagnetic fluids and placed in magnetic fields, are of immense interest due to the rapid, large and tunable transformations in their mechanical and rheological properties. Having in mind the numerous applications [14], a scientific challenge is to investigate which kind of assembled structures are realized depending on combined static and oscillating magnetic fields.

In a typical MR system consisting of superparamagnetic microbeads the induced magnetic moment of a single bead $\mathbf{m}_b = \mathbf{M}_b V_b$, with $V_b = (4\pi/3)d^3$ its volume and \mathbf{M}_b its magnetization, is proportional to the applied external magnetic field \mathbf{H}_0 i.e. $\mathbf{m}_b = \chi_b V_b \mathbf{H}_0$. Here, $\chi_b (> 0)$ stands for the shape-dependent *bead susceptibility* with respect to the external field. This one should not be confused with the material susceptibility $\chi_{b,m} (> \chi_b)$, which characterizes the physical properties of the material itself (not the shape) out of which the bead is made. In the case when the bead is suspended in a solvent with a material susceptibility χ_s in the magnetostatic limit χ_b is given from $\chi_{b,m}$ by [15, 16]

$$\chi_b = 3 \frac{\chi_{b,m} - \chi_s}{3 + \chi_{b,m} + 2\chi_s}. \quad (1)$$

In the following we will study dipolar magnetic (dielectric) beads, which do not carry permanent moments [17]. The beads, enumerated by an index i , are assumed to be all identical, magnetically isotropic and spherically shaped. They are placed in a spatially and temporally fluctuating magnetic field $\mathbf{B}_{0,i} = \mu_0 \mathbf{H}_{0,i}(t)$ with μ_0 the vacuum permeability. We will focus here on the case when the field varies on an intermediate timescale $\tau_H = 2\pi/\omega$ fulfilling the condition $\tau_M \ll \tau_H \ll \tau_{visc}$. Here τ_M is the typical magnetic relaxation time of the paramagnetic bead, which is typically in the range of a 10th of second to microseconds. The other relevant characteristic time scale is the aggregation time $\tau_{visc} \propto \eta$ which characterizes the bead's motion in the surrounding viscous fluid over characteristic distances comparable or larger than the bead diameter d . Under these conditions the beads' magnetization \mathbf{M}_i is equilibrated much faster than its positional coordinate $\mathbf{R}_i(t)$, the beads move and aggregate slowly and feel a net time-averaged force due to the dipole-dipole interaction. In general, the susceptibility $\chi_b(\omega)$ can be a complex frequency dependent function but in the following we will restrict ourselves to the case when $\text{Im} \chi_b(\omega) \ll \text{Re} \chi_b(\omega)$. In this case, the magnetic dissipation effects are in the first approximation negligible compared to the magnetic free-energy effects.

In general, the dynamics of the i -th bead is determined by the interplay of: (1) the friction force $\mathbf{F}_v = -\xi \mathbf{v}_b$ with the friction coefficient $\xi = 6\pi d_b \eta$, (2) the average dipole-dipole force $-\partial \bar{\mathcal{F}}(\mathbf{H}_0, \mathbf{M}_i, \{\mathbf{R}_i\}) / \partial \mathbf{R}_i$ (with the dipole-dipole energy $\bar{\mathcal{F}}(\mathbf{H}_0, \{\mathbf{R}_i\})$) and (3) the fluctuating Brownian force $\mathbf{F}_{B,i}$. However, in the following we shall consider the (quasi-)equilibrium structures first, and postpone the bead dynamics to later works.

The first concrete instance of the cVdW interaction was realized [8–10] a MR suspension that was placed in a magnetic field rotating with a frequency ω on a cone with the opening angle θ , i.e. $\mathbf{H}_0(t) = \sqrt{3} H_0 (\sin \theta \cos \omega t, \sin \theta \sin \omega t, \cos \theta)$ - see Fig. 3a. More precisely, an ideal, fully isotropic cVdW interaction is only realized when the cone opening angle coincides with the magic angle $\theta = \arccos(1/\sqrt{3}) \approx 54.7^\circ$. Such a *balanced triaxial magnetic field* (BTMF) has very special correlation properties: Its components have time averaged correlations, denoted by $\overline{(\dots)}$,

$$\overline{H_{i,0}^\alpha H_{j,0}^\beta} = \delta_{\alpha\beta} H_0^2. \quad (2)$$

that are formally (square) isotropic. Note, that this relation is true even though the BTMF itself has a preferred orientation along the positive z axis, see Fig. 3a. In the most general case we can consider any field realization with such an isotropic correlation property and all particular realizations (cf. Fig. 3(a-b)) will be considered equivalent within our theory. In fact we will abstract away from any concrete representation of the field and take the squared isotropy Eq.(2) as the defining property of the exciting field.

Note that in the most general case found in literature [8],[9] the triaxial field is unbalanced and can have an ar-

bitrary in-plane H_{\parallel} and perpendicular component H_{\perp} : $\mathbf{H}_0 = (H_{\parallel} \cos \omega t, H_{\parallel} \sin \omega t, H_{\perp})$ with $2H_{\parallel}^2 + H_{\perp}^2 = H_0^2$. One can show that in this case the interaction can be linearly decomposed into a balanced triaxial field (BTMF) magic angle interaction and a residual dipole-dipole interaction along the orthogonal direction [7]. The latter is well understood while the former is new and investigated here.

III. THE CVdW FREE-ENERGY

In this section we develop the mathematical formalism necessary to understand the cVdW interaction. The cVdW interaction is a general phenomenon going beyond the magnetic realm and the theory developed here is equally valid for electrically polarizable colloids, i.e. the electrorheological materials. In order to keep the continuity with Refs. [7–10], we arbitrarily follow the magnetic notation. The results for electrically polarizable colloids are obtained by replacing the magnetic quantities with the corresponding electric ones.

Under the condition of quick variations of the external field \mathbf{H}_0 , yet a much quicker equilibration of the magnetization \mathbf{M}_i we study equilibrium structures which minimize the effective (time averaged) free-energy $\bar{\mathcal{F}}$, i.e.

$$-\frac{\partial \bar{\mathcal{F}}(\mathbf{H}_{i,0}, \mathbf{M}_i, \{\mathbf{R}_i\})}{\partial \mathbf{M}_i} = 0 \quad (3)$$

for fixed particle positions \mathbf{R}_i .

In the following we will be dealing with purely athermal effects. This is usually well justified: due to the large moments \mathbf{m}_i of the beads with diameters $D(=2d) > 1 \mu\text{m}$, the energy per particle will be well in excess of the thermal energies making contributions of a configurational entropy negligible in practice. Therefore, all external field fluctuations will be considered as extrinsically given.

The basic expression for the non-equilibrium free-energy $\mathcal{F}\{\mathbf{M}_i, \mathbf{H}_{i,0}(t)\}$ of magnetic colloids (beads) with respect to \mathbf{M}_i in inhomogeneous external time-dependent field $\mathbf{H}_{i,0}(t)$ can be written as [15]

$$\frac{\mathcal{F}}{\mu_0 V_b} = \sum_{i=1}^N \left(\frac{\mathbf{M}_i^2}{2\chi_b} - \mathbf{M}_i \mathbf{H}_{i,0} \right) + \frac{1}{2} \sum_{i,j \neq i} \mathbf{M}_i \hat{T}_{ij} \mathbf{M}_j, \quad (4)$$

where V_b is the bead-volume of one of the N identical beads. $\mathbf{M}_i = \mathbf{m}_i/V_b$ is the magnetization of the i -th bead resulting from its magnetic moment \mathbf{m}_i and χ_b is the *bead (sample) susceptibility* in the external field. The first term in Eq.(4) is the "self-energy" of the beads. It ensures that in absence of external fields there is no magnetization. The second term represents the i – th bead's dipole-dipole interaction with all the other beads. It is

mediated by the dipole tensor \hat{T}_{ij}

$$\hat{T}_{ij} = \varphi_{ij} \hat{t}(\mathbf{b}_{ij}), \quad \varphi_{ij} = \frac{V_b}{4\pi |\mathbf{R}_{ij}|^3} \quad (5)$$

$$\hat{t}(\mathbf{b}_{ij}) = \hat{1} - 3 |\mathbf{b}_{ij}\rangle \langle \mathbf{b}_{ij}|, \quad \mathbf{b}_{ij} = \frac{\mathbf{R}_{ij}}{|\mathbf{R}_{ij}|},$$

with $\mathbf{R}_{ij} \equiv \mathbf{R}_i - \mathbf{R}_j \neq 0$ ($i \neq j$) and \mathbf{b}_{ij} the normalized bonding vector, i.e. the unit vector pointing from bead j to i . Here, we decompose conveniently the dipole tensor \hat{T}_{ij} into a purely geometric 3×3 tensor $\hat{t}(\mathbf{b}_{ij})$ - a linear combination of the unity matrix $\hat{1}$ and the pure projector on the bonding vector $|\mathbf{b}_{ij}\rangle \langle \mathbf{b}_{ij}|$ (in the "Bra-ket" notation). The second contribution in \hat{T}_{ij} is the purely distance dependent dipolar field-decay factor $\varphi_{ij}(R_{ij}) \propto R_{ij}^{-3}$.

Performing the minimization of \mathcal{F} w.r.t. \mathbf{M}_i and reintroducing the result into Eq.(4) we arrive at the quasi-equilibrium free-energy for fixed coordinates $\{\mathbf{R}_i\}$ [15]

$$\mathcal{F}\{\mathbf{H}_{i,0}\} = -\frac{1}{2} \mu_0 V_b \sum_i \mathbf{M}_i \mathbf{H}_{i,0}, \quad (6)$$

where the quasi-equilibrium magnetization of the i -th bead $\mathbf{M}_i(t) = \chi_b \mathbf{H}_{i,loc}(t)$ is determined by the *total local* fields $\mathbf{H}_{i,loc}$ acting at the position of the bead i . These local fields are given implicitly as a function of the applied external fields $\mathbf{H}_{i,0}(t)$ via

$$\sum_j \left(\delta_{ij} + \chi_b \hat{T}_{ij} \right) \mathbf{H}_{j,loc}(t) = \mathbf{H}_{i,0}(t). \quad (7)$$

The last line is strictly valid if we adopt the practical convention that $\hat{T}_{ii} = 0$ for two identical bead indices, i.e. excluding a self-interaction of beads. By inverting Eq.(7), the formal solution for the local fields $\mathbf{H}_{i,loc}$ reads

$$\mathbf{H}_{i,loc} = \chi_b^{-1} \sum_j \hat{\chi}_{eff,ij} \mathbf{H}_{j,0} \quad (8)$$

Here we encounter a main player in the cVdW interaction - the *effective non-local microscopic susceptibility tensor* defined as:

$$\hat{\chi}_{eff} = \chi_b (\hat{1} + \chi_b \hat{T})^{-1}. \quad (9)$$

This *non-local microscopic susceptibility tensor* $\hat{\chi}_{eff}$ is crucial for understanding all the many body effects that will follow. Lets take a few notes in order to understand some of its features. Mathematically, it is a $3 \times N$ - dimensional matrix, relating the external fields at all particle j – th locations to the local fields at particle i – th position. For any fixed i and j , the single components $\hat{\chi}_{eff,ij}$ are themselves 3 dimensional second-rank tensors - i.e. 3×3 matrices in 3-dimensional space. In the following, dealing with $\hat{\chi}_{eff}$ and its components will be conceptually easy with a small caveat and the note of caution:

the i, j components $\hat{\chi}_{eff,ij}$ are to be evaluated *after* performing the operator inversion in Eq. (9). This is at the very origin of the many body forces (cf. below).

With all these issues and precautions about $\hat{\chi}_{eff}$ in mind we can now insert Eq.(8) into Eq.(6) and average over the fluctuating fields $\mathbf{H}_{i,0}(t)$ to obtain the averaged free-energy $\bar{\mathcal{F}}$

$$\begin{aligned}\bar{\mathcal{F}}(\mathbf{H}_0, \{\mathbf{R}_i\}) &= -\frac{\mu_0}{2} V_b \sum_{i,j} \overline{\mathbf{H}_{i,0} \hat{\chi}_{eff,ij} \mathbf{H}_{j,0}} \\ &= -\frac{\mu_0}{2} V_b \sum_{i,j,\alpha,\beta} C_{ij}^{\alpha\beta} \chi_{eff,ij}^{\alpha\beta},\end{aligned}\quad (10)$$

where $C_{ij}^{\alpha\beta}$ is the *field-field correlation function* defined by

$$C_{ij}^{\alpha\beta} = \overline{H_{i,0}^\alpha H_{j,0}^\beta}. \quad (11)$$

Here, $\alpha, \beta = x, y, z$ stand for the 3-spatial directions and $i, j = 1, 2, \dots, N$ are the particle indices. The Eq. (10) is completely general and forms the backbone for all further analysis. It holds both for the classic VdW interaction (with appropriately chosen $\mathbf{H}_{i,0}$) as well as for cVdW and generally couples the field correlators $C_{ij}^{\alpha\beta}$ with the many-body interaction-encoding susceptibility $\chi_{eff,ij}^{\alpha\beta}$ functions. The former are given by the type of interaction (VdW or cVdW) while the latter depend on the spatial configuration of all particles in an interesting but (for now) very convoluted, little transparent manner that we want to elucidate in the following.

A. Incoherent vs. Coherent Fields

The decomposition of the free energy in Eq. (10) into an "external influence" term (the field correlator $C_{ij}^{\alpha\beta}$) and an "internal response" function (susceptibility tensor components $\chi_{eff,ij}^{\alpha\beta}$) is conceptually appealing. The remainder of the paper we will spend on exploring the physical features associated with these two terms.

In a first step, let us investigate how different types of driving field correlations change the interactions. There are two important limiting cases for the correlator $C_{ij}^{\alpha\beta}$:

(A) *strong correlations* with perfect spatial coherence and

(B) *no correlations* in the driving field with perfect decoherence.

These are defined in the following way:

(A) The *spatially coherent fluctuation interaction* with the correlator

$$C_{ij}^{\alpha\beta} = C^{\alpha\beta} = \delta_{\alpha\beta} H_0^2 + h^{\alpha\beta} \quad (12)$$

The first term $C_0^{\alpha\beta} = \delta_{\alpha\beta} H_0^2$ describes the *isotropic* and spatially coherent (uniform) excitation, while the second,

$h^{\alpha\beta}$, describes a uniform constant field (anisotropic contribution). In the following we restrict ourself only to the *isotropic coherent van der Waals interaction* (the cVdW one) with a vanishing anisotropic component, $h^{\alpha\beta} = 0$ i.e.

$$C_{ij}^{\alpha\beta} = C_0^{\alpha\beta} = \delta_{\alpha\beta} H_0^2. \quad (13)$$

It is easy to see that the corresponding *cVdW free-energy*, is then given by

$$\bar{\mathcal{F}}_{cVdW}(\mathbf{H}_0, \{\mathbf{R}_i\}) = -\frac{\mu_0}{2} H_0^2 V_b \sum_{i,j} \text{Tr}(\hat{\chi}_{eff,ij}), \quad (14)$$

where

$$\text{Tr}(\hat{\chi}_{eff,ij}) \equiv \chi_{eff,ij}^{xx} + \chi_{eff,ij}^{yy} + \chi_{eff,ij}^{zz} \quad (15)$$

is the trace of the effective susceptibility. Note, that the coherent isotropic correlation function $C_{\alpha\beta} = \delta_{\alpha\beta} H_0^2$ comprises also the case of the experimentally realized *balanced triaxial magnetic fields* [8–10] (BTMF) - see *Section II* and Fig.3a. Even though the cone at which the field precesses has a direction (opening) by itself, the square of the field is statistically identical in all directions and mutually uncorrelated in all directions i.e. $\overline{H_{i,0}^\alpha H_{j,0}^\beta} = \delta_{\alpha\beta} H_0^2$. The BTMF is therefore only one instance of a general coherent isotropic field. Any other realization, like e.g. one of those in Fig 3b satisfies the relation (10) and consequently has the same energy Eq. (13).

(B) The *spatially incoherently excited fields* are realized for $C_{ij}^{\alpha\beta} = \delta_{ij} C^{\alpha\beta}$. The latter may in principle contain isotropic and anisotropic terms, too. Note, that the term proportional to δ_{ij} means that the correlations of magnetic field fluctuations on different particles vanish. In the completely *isotropic* case one has

$$C_{ij}^{\alpha\beta} = \delta_{ij} \delta_{\alpha\beta} H_0^2 \quad (16)$$

and the fully incoherent VdW free-energy - of the *VdW systems*, reads

$$\bar{\mathcal{F}}_{VdW}(\mathbf{H}_0, \{\mathbf{R}_i\}) = -\frac{\mu_0}{2} H_0^2 V_b \sum_i \text{Tr}(\hat{\chi}_{eff,ii}). \quad (17)$$

Note, that there is a *significant difference* between the two excitation cases (A) and (B), described by Eq.(14) and Eq.(17), respectively. In the incoherent case (B) the free-energy $\bar{\mathcal{F}}_{VdW}(\mathbf{H}_0, \{\mathbf{R}_i\})$ contains a summation over the index i only, i.e. it includes only the diagonal terms $i = j$ - sometimes called the self-energy terms. This is equivalent to the usual Van der Waals (VdW) interaction and in the following this part of the free-energy will be called the VdW one. However in the novel case (A) $\bar{\mathcal{F}}_{cVdW}$ contains the more complex, double summation over i and j which gives rise to unusual, non-local and anisotropic many body effects in cVdW system - most of which are absent in a standard VdW system (case B).

In the coherent case, the terms $Tr(\hat{\chi}_{eff,ij})$ with $i \neq j$, describe the effective coupling between the i -th and j -th bead acting directly or indirectly via all other beads, thus giving rise to very specific and anisotropic *many body interactions*. The latter will turn out to be a crucial effect for cVdW matter and will be responsible for the formation of hierarchical assemblies of colloids. This is in strong contrast with the standard VdW systems where 3D bulk structures such as droplets and close-packed 3D crystal structures are favored and realized.

IV. MICROSCOPIC CVDW THEORY - MANY BODY INTERACTIONS, THE FORMATION OF CHAINS AND MEMBRANES

In this Section we will explore how a *microscopic cVdW theory*, based on the effective energy Eq.(14) and the non-local many body susceptibility Eq.(9) works in practice. While the energy Eq.(14) appears (deceptively) straightforward to evaluate, the many body susceptibility operator Eq.(9) is a sophisticated mathematical object. To grasp physical insights about the latter, except for the simplest case of two spherical beads, seems challenging.

After dealing with the elementary case of two particles, which can be treated exactly, we will resort to the approximation of small bead susceptibility i.e. $\chi_b \ll 1$ - a limiting case that allows a controllable evaluation of the many body interactions. In this spirit we will be making an energy expansion up to lowest order in χ_b . Notably, this lowest order expansion of the energy, as we will see, comprises both the 2-body interaction of beads and the non-local 3-body interactions at the same order.

As it will be shown both these interactions (2 and 3 body) scale identically with distance for cVdW, i.e. $\bar{\mathcal{F}}_{2-body} \propto \bar{\mathcal{F}}_{3-body} \propto R^{-6}$. The *2+3 body inseparability* is the most peculiar *hallmark signature of the cVdW interaction*, and to our knowledge stands out rather uniquely among other known many-body forces in Nature.

A. Two-Body Interaction - Dimer Formation

Let us start out elementary and consider a very dilute system. In such a case the *pairwise* bead-bead (2-body) interaction should dominate in the free-energy $\bar{\mathcal{F}}_{cVdW}$. While this assumption of dominant 2-body forces turns out as too naive (see the next subsection) it is still natural to consider only two interacting particles first. For two beads 1 and 2 the non-local susceptibility operator $\hat{\chi}_{eff}$ is easily calculated by using Eq. (9). The detailed derivation is given in *Appendix 1A* while the final result reads

$$Tr\hat{\chi}_{eff} = C \cdot \begin{pmatrix} 1 - 3\varphi_{12}^2\chi_b^2 & 2\chi_b^3\varphi_{12}^3 \\ 2\chi_b^3\varphi_{12}^3 & 1 - 3\varphi_{12}^2\chi_b^2 \end{pmatrix} \quad (18)$$

$$C = \frac{3\chi_b}{(1 - 4\varphi_{12}^2\chi_b^2)(1 - \varphi_{12}^2\chi_b^2)} \quad (19)$$

Having the trace of $\hat{\chi}_{eff}$, we can now evaluate the mean free energy for the incoherent and the coherent case.

In the *incoherent (standard) VdW* case the energy $\bar{f}_{VdW} = \bar{\mathcal{F}}_{VdW} / (\mu_0 V_b H_0^2)$ is the sum of the $Tr\hat{\chi}_{eff}$ diagonals (note $(Tr\hat{\chi}_{eff})_{11} = (Tr\hat{\chi}_{eff})_{22}$) i.e.

$$\begin{aligned} \bar{f}_{VdW} &= -(Tr\hat{\chi}_{eff})_{11} \\ &= -\frac{3\chi_b(1 - 3\varphi_{12}^2\chi_b^2)}{(4\varphi_{12}^2\chi_b^2 - 1)(\varphi_{12}^2\chi_b^2 - 1)}. \end{aligned} \quad (20)$$

On the other hand, for the *coherent cVdW* interaction we have to sum all four elements of $Tr\hat{\chi}_{eff}$ (note $(Tr\hat{\chi}_{eff})_{12} = (Tr\hat{\chi}_{eff})_{21}$) obtaining

$$\begin{aligned} \bar{f}_{cVdW} &= -(Tr\hat{\chi}_{eff})_{11} - (Tr\hat{\chi}_{eff})_{12} \\ &= -\frac{3\chi_b(1 - \chi_b\varphi_{12})}{(1 + \chi_b\varphi_{12})(1 - 2\chi_b\varphi_{12})}. \end{aligned} \quad (21)$$

Interestingly, the coherent and the incoherent 2 bead interaction energy look very similar but are *not* identical. After expanding the energies in powers of φ_{12} we see that $\bar{f}_{VdW} = -3\chi_b - 6\varphi_{12}^2\chi_b^3 - 18\varphi_{12}^4\chi_b^5 + \dots$ and $\bar{f}_{cVdW} \approx -3\chi_b - 6\varphi_{12}^2\chi_b^3 - 6\varphi_{12}^3\chi_b^4 + \dots$ or in terms of the bead-bead distance R_{12} :

$$\begin{aligned} \bar{f}_{VdW} &\approx -3\chi_b - \frac{3V_b^2\chi_b^3}{8\pi^2}R_{12}^{-6} - \frac{9\chi_b^5V_b^4}{128\pi^4}R_{12}^{-12} \\ \bar{f}_{cVdW} &\approx -3\chi_b - \frac{3V_b^2\chi_b^3}{8\pi^2}R_{12}^{-6} - \frac{3V_b^3\chi_b^4}{32\pi^3}R_{12}^{-9} \end{aligned} \quad (22)$$

We observe that the first interaction terms $\propto R_{12}^{-6}$ exactly coincide. This interesting 2-body result was first obtained by Martin and coworkers [8, 9] and confirmed experimentally by Osterman et al. [10]. However, the higher order terms in \bar{f}_{VdW} and \bar{f}_{cVdW} scale quite differently, and they are $\propto R_{12}^{-12}$ and $\propto R_{12}^{-9}$, respectively. This makes the cVdW interaction slightly stronger (more attractive) than the usual incoherent VdW.

Now, if it was only for this slight difference between the two, investigating the cVdW would hardly be very interesting. But we will see soon that the 3-body forces are a real game changer, giving the cVdW interaction its unique character and flavor.

B. Many Body Interactions

For the standard (incoherent) VdW interaction the 2-body interaction is $\propto |\mathbf{R}_{12}|^{-6}$ in leading order and since

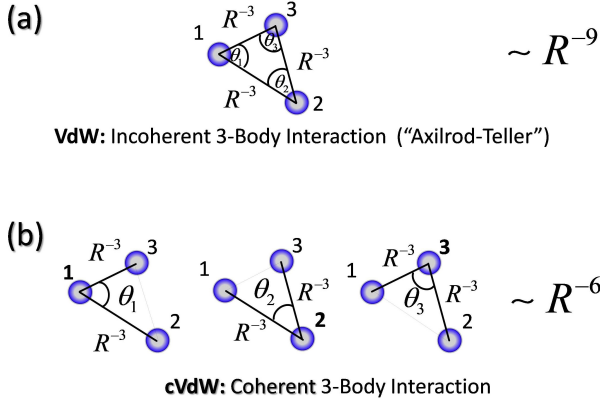


FIG. 4: The 3-body forces of (a) the incoherent (VdW) and (b) the coherent (cVdW) interaction have different angular character and are longer ranged for cVdW, Eq.(29).

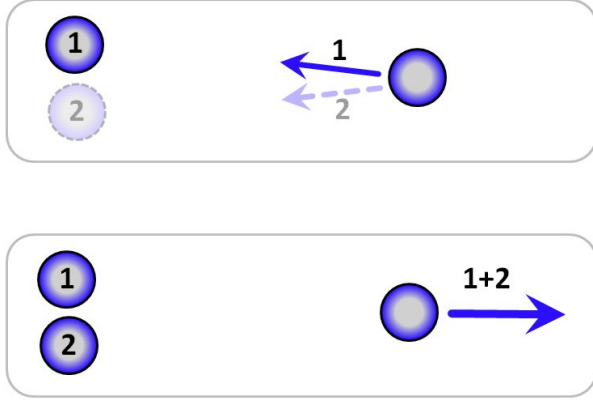


FIG. 5: Top - The most surprising consequence of the cVdW 3-body nature: Bead 1 and bead 2 individually (if alone) attract the bead 3 on the right. Bottom - However when placed together beads 1+2 repel the bead 3 due to a strong 3-body force.

the 3-body (and higher order) interactions are shorter ranged (cf. below) and much smaller in magnitude than the 2-body ones, VdW favors the formation of close packed droplet-like or 3D bulk (crystalline) structures with high symmetries [13]. If the 2-body interaction - given by Eq.(22) - would dominate the behavior of cVdW as well, one would also expect the formation of bulk droplets. However this is in sharp contrast to experimental evidence [8–10] which shows a clear *tendency for chain and membrane formation*, i.e. for low-dimensional structures under cVdW. What is the microscopic origin of these complex and low dimensional (anisotropic) structures in cVdW systems?

In the following we will explore how this remarkable difference of the two forces emerges once the three body forces are considered.

To this end we consider the free energy Eq.(14) with

Eq.(9) in the general case of $N \geq 3$ particles. We expand the non-local susceptibility tensor $\chi_b(\hat{1} + \chi_b \hat{T})^{-1}$ for small bead susceptibility and large distances $\chi_b \varphi_{ij} \ll 1$ (i.e. $\chi_b \hat{T} \ll 1$) into a Taylor series and take its trace over spacial directions:

$$Tr \hat{\chi}_{eff} = Tr \left(\chi_b \hat{1} - \chi_b^2 \hat{T} + \chi_b^3 \hat{T}^2 - \chi_b^4 \hat{T}^3 + \dots \right) \quad (23)$$

The resulting (scaled) free energy in the coherent case is then $\bar{f}_{cVdW} \equiv \bar{\mathcal{F}}_{cVdW}/(\mu_0 V_b H_0^2) = -\frac{1}{2} \sum_{i,j} Tr(\hat{\chi}_{eff,ij})$ can be split in terms of ascending order in χ_b :

$$\bar{f}_{cVdW} = \bar{f}_{cVdW}^{(1)} + \bar{f}_{cVdW}^{(2)} + \bar{f}_{cVdW}^{(3)} + O(\chi_b^4 \hat{T}^3). \quad (24)$$

with $\bar{f}_{cVdW}^{(k)} \propto \chi_b^k \sum_{i,j} Tr(\hat{T}^{k-1})_{ij}$. Similarly we can expand the incoherent VdW energy in terms like $\bar{f}_{VdW} \propto \chi_b^k \sum_i Tr(\hat{T}^{k-1})_{ii}$ as

$$\bar{f}_{VdW} = \bar{f}_{VdW}^{(1)} + \bar{f}_{VdW}^{(2)} + \bar{f}_{VdW}^{(3)} + \bar{f}_{VdW}^{(4)} + \dots \quad (25)$$

Note that for VdW systems, it is necessary to include the term $\bar{f}_{VdW}^{(4)}$ since this term contains the leading 3-body interaction (Axilrod-Teller interaction - see below) in the Van der Waals case.

To shed light on the difference between cVdW and VdW energies, let us have a closer look at the terms of the expansion Eq.(23). The first term $Tr(\chi_b \hat{1}) = 3\chi_b$ is particle distance independent and describes noninteracting beads, while the second term of Eq.(23) trivially vanishes as the tensors \hat{T}_{ij} are traceless: $Tr \hat{T}_{ij} = \varphi_{ij} Tr(\hat{1} - 3\hat{N}_{ij}) = 0$. Here again $\hat{N}_{ij} = |\mathbf{b}_{ij}\rangle \langle \mathbf{b}_{ij}|$ is the bond vector projector with $Tr(\hat{N}_{ij}) = 1$. It is only the third term of Eq.(23) $\propto Tr(\hat{T}^2)_{ij} = \sum_{k=1}^N \varphi_{ik} \varphi_{kj} Tr[(\hat{1} - 3\hat{N}_{ik})(\hat{1} - 3\hat{N}_{kj})]$ that gives rise to the first non-trivial interaction contribution. Using $Tr[\hat{N}_{ik} \hat{N}_{kj}] = Tr[|\mathbf{b}_{ik}\rangle \langle \mathbf{b}_{ik}| |\mathbf{b}_{jk}\rangle \langle \mathbf{b}_{jk}|] = (\langle \mathbf{b}_{ik} | \mathbf{b}_{jk} \rangle)^2 := \cos^2 \theta_{k,ij}$ which involves the angle $\theta_{k,ij}$ between the bond vectors \mathbf{b}_{ik} and \mathbf{b}_{jk} (at the particle k) we obtain:

$$\left[Tr(\hat{T}^2) \right]_{ij} = 3 \sum_{k=1}^N \varphi_{ik} \varphi_{kj} (3 \cos^2 \theta_{k,ij} - 1) \quad (26)$$

Similarly, using the relation $Tr[\hat{N}_{kl} \hat{N}_{ik} \hat{N}_{lj}] = \cos \theta_{kl,ik} \cos \theta_{ik,lj} \cos \theta_{kl,lj}$ with the angles between the bond vectors defined by $\cos \theta_{ik,jl} = \langle \mathbf{b}_{lj} | \mathbf{b}_{ik} \rangle$ we can expand also the 4-th term $\propto \hat{T}^3$ of Eq.(23):

$$\begin{aligned} \left[Tr(\hat{T}^3) \right]_{ij} &= \sum_{k=1}^N \sum_{l=1}^N \varphi_{ik} \varphi_{kl} \varphi_{lj} C_{iklj} \quad \text{with} \quad (27) \\ C_{iklj} &= 9 (\cos^2 \theta_{ik,jl} + \cos^2 \theta_{ik,kl} + \cos^2 \theta_{jl,lk}) \\ &\quad - 27 \cos \theta_{kl,ik} \cos \theta_{ik,lj} \cos \theta_{kl,lj} - 6 \end{aligned}$$

With these results in our hands we are now well equipped to analyze the 3-body terms of the two interactions, cVdW and VdW, and understand how they differ.

1. 3-Body Energy for the Incoherent VdW

From the $Tr(\hat{T}^2)$ term given by Eq.(26) we obtain the incoherent 2-body interaction $\bar{f}_{VdW}^{(3)} = -3\chi_b^3 \sum_{i,k} \varphi_{ki}^2$. To calculate the lowest order VdW 3-body term $\bar{f}_{VdW}^{(4)}$ we define in the triangle (ikl) the angles $\theta_i, \theta_k, \theta_l$ - cf. Fig.4a, with the properties $\cos \theta_{i,kl} = -\cos \theta_i$, etc. By using the geometrical rule $\cos^2 \theta_i + \cos^2 \theta_k + \cos^2 \theta_l = 1 - 2 \cos \theta_i \cos \theta_k \cos \theta_l$ for a triangle we obtain

$$\bar{f}_{VdW}^{(4)} = \frac{1}{2} \sum_{i,k,l} \varphi_{ik} \varphi_{kl} \varphi_{li} C_{ikl} \quad (28)$$

$$C_{ikl} = 3(3 \cos \theta_i \cos \theta_k \cos \theta_l + 1).$$

This term coincides exactly with the *Axilrod-Teller 3-body potential* [18] for the Van der Waals interaction. Due to its weaker ($\sim R^{-9}$) scaling than the 2-body force, it is typically *small and overridden* by the 2-body VdW interaction $\sim R^{-6}$ [19] giving rise to close packed structures and droplets in VdW systems.

2. The cVdW 3-Body Energy

In the case of the cVdW interaction the effective free-energy is given by Eq.(14) where the double summation over i, j must be performed by including $i = j$, as well. The presence of non-local terms with $i \neq j$ gives rise to qualitatively new many-body effects in cVdW matter with respect to the VdW one. As seen from Eq.(26), the leading 3-body cVdW interaction term arises from $\bar{f}_{cVdW}^{(3)}$ and is thus proportional to \hat{T}^2 , so it scales as $\propto \chi_b^3 R^{-6}$. This means that the leading order 3-body cVdW interaction term is of the same order as the 2-body cVdW one [20]. The *3-body free-energy* $\bar{f}_{cVdW}^{(3)}$ is given by

$$\bar{f}_{cVdW}^{(3)} = -\bar{\beta} \sum'_{i,j,k} \frac{3 \cos^2 \theta_{k,ij} - 1}{|\mathbf{R}_{ik}|^3 |\mathbf{R}_{kj}|^3}, \quad (29)$$

where $\bar{\beta} = (3/32\pi^2)\chi_b^3 V_b^2$ and the sum running over all triplets (i, j, k) with $k \neq i, j$ (for angles $\theta_{k,ij}$ cf. Fig.4b).

Since the 2-body interaction in cVdW systems is *contained* in $\bar{f}_{cVdW}^{(3)}$ (for $k \neq i = j$) it is physically *inseparable from the 3-body one*. Therefore the 3-body interaction must be treated on the same footing as the 2-body one. This fact shows us the pitfall in the dimer formation section which considered the 2-body interaction alone. Interestingly, $\bar{f}_{cVdW}^{(3)}$ in Eq.(29) is very anisotropic and has

a specific angular dependence. This angular dependence intuitively hints towards the explanation of the tendency of cVdW interaction not to form 3D bulk structures, but to drive the formation of anisotropic 1D and 2D structures. For instance, the $-\cos^2 \theta_{k,ij}$ term in $\bar{f}_{cVdW}^{(3)}$ favors either $\theta_{k,ij} = 0$ or π - i.e. a colloidal chains, membranes are preferred by the many body interactions.

C. The Principle of "Anisotropic Lumping": An Emergent 2-Body Interaction from the 3-Body One

In this section we investigate how the 3-body cVdW interaction works in a simple physical limit. Let us consider only 3 beads and place two of them, say 1 and 2, very close to each other at distance $R_{12} = r$, while the bead number 3 is at large distance from 1 and 2, i.e. we assume $R_{13} \approx R_{23} \approx R \gg r$. The free-energy Eq.(29) is calculated in *Appendix 2A* and the expression up to the lowest order in the distance is

$$\frac{\bar{f}_{cVdW}^{(3)}}{\beta} = -\frac{4}{r^6} - \frac{4(3 \cos^2 \theta_{3,12} - 1)}{r^3 R^3} + O(R^{-6}), \quad (30)$$

where the first term is the 2-body interaction between particles 1 and 2. The peculiarity of the second term in Eq.(30), i.e. the three-body interaction is readily seen, when two particles are very near and the third one is far away. From Eq.(30) it comes out that for the bead arrangement shown in Fig.5, although the two body interactions 1-3 and 2-3 are attractive, the third bead is repelled from the first two as a consequence of the anisotropic 3-body interactions. This is due to the condition $R \gg r$ making $\cos^2 \theta_{3,12} \ll 1$ for $\theta_{3,12} \approx \pi/2$ in the configuration of Fig. 5.

The second interesting observation that we can make from Eq.(30) is that for a fixed dimer size r , the third particle interacts with the point-like two particle complex via a "long-range" force $\propto R^{-3}$. The 1+2 dimer, instead of the two single monomers becomes now the emerging elementary unit governed by different laws than single particles.

This example is quite instructive and tells us a lot about the very nature of cVdW. On the one hand particles display many-body effects which override their individual pairwise interaction in most general configurations. However there is another idea emerging from the same example, which simplifies dealing with the cVdW quite a bit. When two beads come together - i.e. "lump" together by attractive forces - and find themselves much closer then to the rest of the beads, they can be considered as a new combined entity- the dimer. Now, the dimer itself interacts with the rest of the world by an anisotropic, angle dependent, longer ranged interaction $\propto R^{-3}$ (instead of R^{-6}), and this interaction is now 2-body, pairwise and is attractive for $3 \cos^2 \theta_{3,12} - 1 > 0$.

The concept of "lumping" works generally, also for more than 3 particles which are forming anisotropic lumps out of closely packed aggregates of particles. The

usefulness of the lumping idea will become more clear in sections that will follow. In particular, we will derive how beads lumped together inside of chains or membranes interact with other beads and other lumps in the far field. The consideration of the pairwise interactions of such lumps, instead of all many-body interactions of all particles, will be an enormous simplification.

D. Anomalous Elasticity of cVdW Chains and Membranes

Here we study consequences of the many body effects in cVdW chains and membranes with finite number (N) of particles, - called finite N-effects. Additionally, we study their unusual elastic properties and compare with more classical systems with short range forces. In order to grasp the physics of the problem in the simplest form, we calculate the free-energy for small bead susceptibility, $\chi_b \ll 1$ - see Eq.(29), which includes first non-trivial and leading 3-body effects.

1. 3-Body Effects in cVdW Chain - Free-Energy and Elasticity

(i) *Finite linear chain* - The free-energy per particle of the finite chain $\bar{f}_{cVdW,ch}^{(3),N} (\equiv \bar{\mathcal{F}}_{cVdW,ch}^{(3)}/N)$ is calculated by direct summation of 3-body forces in *Appendix 2B* and the result is

$$\frac{\bar{f}_{cVdW,ch}^{(3),N}}{\beta} \approx -\frac{8\zeta^2(3)}{D^6} + \frac{3.4}{ND^6}, \quad (31)$$

with $\beta = (3/32\pi^2)\mu_0 H_0^2 \chi_b^3 V_b^3$ and the zeta function $\zeta(3) \simeq 1.2$. The first $O(1)$ term is the free-energy per particle of an infinite chain, while the leading finite N term is of order $O(1/N)$. The latter is the price the last few edge particles (at both free ends) pay for being at the end of the chain. Note that, this edge energy being positive indicates that the chain would like to be closed eventually (i.e. eliminate free ends), provided that the bending energy for doing so is less than the gained edge energy.

(ii) *Young's modulus for linear chain* - If one generates a slight increase of the distance D between bead centers, i.e $D \rightarrow D(1 + \varepsilon)$ then the Young's modulus of the stretched chain can be formally defined by the second derivative of the free energy like $Y(\varepsilon = 0) = -(1/DS_b)(\partial^2 \bar{\mathcal{F}}_{cVdW,ch}^{(3)}/\partial \varepsilon^2)$, where the bead cross-section surface is $S_b \simeq \pi(D/2)^2$. From Eq.(31) one obtains

$$Y(\varepsilon = 0) \approx 0.84 \cdot \mu_0 H_0^2 \chi_b^3,$$

i.e. the effective Young's modulus scales quadratically with external field (for small χ_b) and is independent of the bead diameter D . For $\chi_b > 0$ (paramagnetic beads)

it is of course $Y(\varepsilon = 0) > 0$, which guarantees stability of the chain. In case of $\chi_b < 0$ (effective diamagnetic beads - when the medium susceptibility $\chi_m > \chi_b$) one has $Y(\varepsilon = 0) < 0$ and the chain is unstable due to the repulsive forces of effectively diamagnetic beads.

(iii) *Bending energy of ring* - In another situation, instead of stretching the chain, we can bend its center line and close it into a ring. The free-energy per particle in this case is calculated in *Appendix 2C* and reads

$$\frac{\bar{\mathcal{F}}_{cVdW,ring}^{(3)}}{N\beta} \approx -\frac{8\zeta^2(3)}{D^6} + \frac{16\pi^2\zeta(3)\ln N}{D^6 N^2}. \quad (32)$$

The first (leading) term is the same as for the infinite linear chain, while the second term in Eq.(32) can be related to the bending elasticity energy per particle of the coherent VdW chain. Usually, the bending modulus (stiffness) K for the chain with short range forces is defined as the prefactor in the bending energy

$$\bar{\mathcal{F}}_{bend,ring} - \bar{\mathcal{F}}_{ch} = \frac{K}{2} \int_0^{2\pi R} ds \left(\frac{\partial \mathbf{t}}{\partial s} \right)^2 = K \frac{\pi}{R}. \quad (33)$$

where the latter is true for a ring. Here, \mathbf{t} is the unit tangent vector $\mathbf{t} = (-\cos(s/R), \sin(s/R), 0)$ and $R = ND/2\pi$.

By interpreting the cVdW ring in this elasticity framework a first surprise comes out. From Eq.(32) and Eq.(33) we see an anomalous behavior of the effective bending modulus

$$K_{cVdW} \simeq \frac{\zeta(3)D}{48} (\mu_0 H_0^2 \chi_b^3 V_b) \ln N, \quad (34)$$

i.e. $K_{cVdW} \propto \ln N \propto \ln R/D$ grows logarithmically with the chain size. This behavior is qualitatively very different from the case of the chain with short range interaction, where K is always a N-independent constant. The logarithmic stiffness of chains is caused by the long-range many body nature of cVdW.

It is interesting to note that even though the bending stiffness is growing, the chain closure cost (per bead) $\propto N^{-2} \ln N$ is becoming quickly smaller with large N . A comparison of the ring energy Eq.(32) with the straight chain result Eq.(31) tells us that the rings will indeed become more preferable for long enough chains with $N \gtrsim 320$.

2. cVdW Membranes - Free-Energy and Elastic Properties

As in the case of linear chains we can consider the elastic and finite size properties of flat and curved membranes. Most of the results in this section can be derived from the phenomenological macroscopic (demagnetization tensor) approach for fat cylinders, hollow spheres etc. presented in the forthcoming sections, while others are obtained by discrete summations. Here we only

present the main physical results and point out the unusual size dependent scaling of various material properties.

(i) *The free-energy of the finite flat membrane* - The discrete summations of the free-energy $\bar{\mathcal{F}}_{cVdW,fl-me}^{(3),N}$ for large N and the radius $R \propto \sqrt{N}$ are difficult due to absence of a convenient symmetry for all particles (like present for the ring). However, if we combine the results for the tubular membrane in the limit $N \rightarrow \infty$ - see Eq.(38) and *Appendix 2E*, with the finite N corrections in the cylindrical scheme 2 of the macroscopic approach - see Eq.(49). In this approach we can estimate $\bar{\mathcal{F}}_{cVdW,fl-me}^{(3),N}$

$$\frac{\bar{\mathcal{F}}_{cVdW,fl-me}^{(3),N}}{N\beta} \approx -\frac{8\pi^4}{27D^6} + \frac{B \ln N}{D^6 \sqrt{N}}, \quad (35)$$

with $B = 192\rho_{pack}^2$. Here, $\rho_{pack} < 1$ is the *packing (volume) fraction* of the beads in membrane. The second term in Eq.(35) is due to the line tension of the membrane. This line tension, similarly as the bending stiffness of chains, scales logarithmically with the system size.

(ii) *Bending energy of the spherical membrane (vesicle)* - For a fluid, spherical membrane of radius R with classical elasticity (due to a finite range interaction) the energy density would be proportional to $(1/R^2)$ (=curvature²). In that case classic "Helfrich-like" membrane case the total energy coming solely from the bending is then $\sim \frac{1}{R^2} R^2 \sim 1$, i.e. it is constant for all vesicle sizes. What happens in the case of a cVdW vesicle? To answer that, we can calculate the 3-body part of the free-energy per particle with the diameter D of the spherical shell - see *Appendix 2D*, which gives

$$\frac{\bar{\mathcal{F}}_{cVdW,sph-me}^{(3),N}}{N\beta} \approx -\frac{50\pi\rho_{sph}^2}{D^6} + \frac{50\sqrt{\pi}\rho_{sph}^{9/4}}{D^6\sqrt{N}}, \quad (36)$$

where $\rho_{sph} \approx 0.4$ is the surface packing factor of the spherical beads on the sphere, obtained by comparing Eq.(36) and Eq.(35). The relation between ρ_{sph} , N and the radius of the shell R is given by $N = 4\pi R^2/\rho_{sph}^{-1}\pi(D/2)^2 (= 16\rho_{sph}R^2/D^2)$. The free-energy expressed in terms of $R(\propto \sqrt{N})$ is given by

$$\frac{\bar{\mathcal{F}}_{cVdW,sph-me}^{(3),N}}{\beta} \approx -const.N + \frac{204\sqrt{\pi}\rho_{sph}^{11/4}}{D^7}R, \quad (37)$$

where the first term is the constant energy per particle. The second term is remarkable as the bending energy grows with radius $\propto R(\propto \sqrt{N})$. This means that the effective bending energy density is $\propto R^{-1}(\propto N^{-1/2})$ which is much larger than in classical membranes where $\propto R^{-2}(\propto N^{-1})$. To put it differently, the bending stiffness of the membrane K_{me} becomes size dependent with $K_{me} \sim \sqrt{N}$. This behavior is also confirmed in the macroscopic theory (studied below) for the continuous hollow sphere.

After the logarithmic stiffness of the chain (with $K_{ch} \propto \ln N$), the non-locality of the bending stiffness of membrane is another signature of the anisotropic and long range 3-body nature of the coherent interaction in cVdW systems. This is somehow reminiscent, of the physics of classic elastic cross-linked (i.e. non-fluid) membranes where the non-locality is due to the coupling of in-plane strains with the flexural deformation [21]. These effects of the elastic in plane coupling are neglected in our case, as the curved cVdW membranes can be considered to be a well shaken, i.e. behaving like a fluid and without in-plane stresses. The size dependent stiffness effects emerge in our case entirely from the many-body, long-range nature of the cVdW interaction.

By comparing the free-energies for the flat- and spherical-membrane in Eq.(35) and Eq.(36) one sees that for finite, but large, N the spherical membrane has lower energy than the flat one, i.e. $\bar{\mathcal{F}}_{cVdW,sph-me}^{(3),N} < \bar{\mathcal{F}}_{cVdW,fl-me}^{(3),N}$. This result is also confirmed in the macroscopic approach - see below. At the first glance this result is not conform with experiments where only flat membranes were observed [8–10]. This can be explained by the fact that, in order to form a spherical membrane large energy barriers, far beyond thermal energies ($\bar{\mathcal{F}}_{cVdW,sph-me}^{(3),N} \gg kT$), have to be overcome. This might prevent the spherical membranes from being observed experimentally, so far.

(iii) *Bending energy of the tubular membrane* - We consider the case when the thickness of the tube is the bead radius D , i.e. $R_2 - R_1 = D$. The approximate free-energy is calculated in *Appendix 2E*. The obtained free-energy in the leading order is given by

$$\frac{\bar{\mathcal{F}}_{cVdW,tub}^{(3)}}{\beta N} \simeq -\frac{8\pi^2}{27} \frac{1}{D^6} (\pi^2 - 5 \frac{D}{R_{\perp}}), \quad (38)$$

where $N = N_1 N_2$, $R_{\perp} \sim N_1$ is the external radius of the tube and the limit $(R_{\perp}/D) \gg 1$ is assumed - see Fig.11. The first nontrivial term is proportional to $1/R_{\perp}$ which means that the tubular membrane (cylindrical shell) has a similar type of anomalous and non-local elasticity (at least in scaling) as the spherical membrane. This result is also confirmed within the macroscopic approach - see the next Subsection.

V. MACROSCOPIC APPROACH TO CVDW

By studying the microscopic 3-body interaction in Eq.(29) we have understood, intuitively and qualitatively, why chains form initially. However, in order to capture quantitatively their transition to membranes for arbitrary values of $\chi_b < 3$, higher $O(\chi_b^4 \varphi_{ij}^4)$ terms beyond the 3-body interactions (in Eq.(29)) are necessary. This appears as a difficult task at present. In order to study the assembly of magnetic colloids, especially in dense systems, hard and physically much less transparent

numerics would be necessary. Therefore, it is conceptually instructive to take a more macroscopic, continuous mean-field approach [15], where *dense chains/membranes* are modelled as a continuum medium. In this approach the dipolar tensor \hat{T}_{ij} is replaced by its macroscopic analogue - the demagnetization tensor \hat{L} , while the microscopic effective susceptibility $\hat{\chi}_{eff,ij}$ in Eq.(9) is replaced in the continuum limit by the corresponding macroscopic, (shape-dependent) tensor-susceptibility $\hat{\chi}^{(L)}$ given by [15]

$$\hat{\chi}^{(L)} = \chi(1 + \hat{L}\chi)^{-1}. \quad (39)$$

Here, χ is the *material susceptibility* (with respect to an internal field \mathbf{H}_{int}) which is due to local field effects in an aggregate of beads and depends in a nonlinear way on the bead susceptibility χ_b . For $\chi_b > 0$ one has $\chi > \chi_b$. The demagnetization tensor \hat{L} depends on the shape of the sample, which is chosen in such a way to mimic the composite structure like e.g. a chain and membrane. The time-averaged cVdW free-energy $\bar{\mathcal{F}}$ in the macroscopic approach is generally given by [7]

$$\bar{\mathcal{F}}^{mac}(\mathbf{H}_0, \hat{L}) = -\frac{1}{2}\mu_0 H_0^2 V Tr \left\{ \hat{\chi}^{(L)} \right\}, \quad (40)$$

together with Eq.(39), where the demagnetization coefficients L_x, L_y, L_z - the eigenvalues of \hat{L} - depend on the shape and aspect ratio of the sample.

As already mentioned the main structures that form on the intermediate scales are initially chains and then membranes. In the macroscopic approach we can model them within the framework of two different schemes:

(1) the *spheroid scheme*, where the structure is replaced with a spheroidal shape with the semi-axes $a = b \neq c$ and the volume $V = (4\pi/3)a^2c$, where we have $c \gg a$ for *prolates (chains)* and $c \ll a$ for *oblates (membranes)*, or

(2) the *cylinder scheme*, where the sample is modelled by a cylinder with height h and radius R . For a *long cylinder* we have $h \gg R$ and $h \ll R$ for a *thin (flat) one*.

It will be shown below that for infinite systems both approaches (1) and (2) give the same results, while for a finite number of particles (the N -effects) they differ. We study also the energetics of the *spherical membrane (spherical shell - coated sphere)* which in the large N limit mimics a membrane and its bending stiffness. At the end of this chapter, we shall also compare the microscopic and macroscopic approach for various shapes and ask for consistency of the two approaches.

A. Infinite Chains and Membranes

Here we consider the case $N \rightarrow \infty$ and obtain asymptotic results for large (infinite) membranes and chains.

(i) *Chain* - The two perpendicular demagnetization factors of infinite chains are given by $L_{a,\infty} = L_{b,\infty} = 1/2$, while for the one along the long chain axis we have

$L_{c,\infty} = 0$ in both schemes (cylinder and ellipsoid). In that case Eq.(40) gives the macroscopic approximation of the free-energy $\bar{\mathcal{F}}_{ch,\infty}^{mac}$ of chain

$$\bar{\mathcal{F}}_{ch,\infty}^{mac}(\mathbf{H}_0) = -\frac{1}{2}\mu_0 H_0^2 V \chi \left(1 + \frac{2}{1 + \chi/2}\right) \quad (41)$$

(ii) *Membrane* - In both schemes in the limit $N \rightarrow \infty$ one has $L_{a,\infty} = L_{b,\infty} = 0$, $L_{c,\infty} = 1$ and the asymptotic free-energy of the membrane is

$$\bar{\mathcal{F}}_{me,\infty}^{mac}(\mathbf{H}_0) = -\frac{1}{2}\mu_0 H_0^2 V \chi \left(2 + \frac{1}{1 + \chi}\right) \quad (42)$$

Note, that for both chains and membranes the macroscopic free-energy is dominated by the smallest demagnetization factors $L^{m/ch} \rightarrow 0$. For membranes two demagnetization factors vanish, while for chains only one vanishes. Then, for $N \rightarrow \infty$ and by assuming the same χ for chains and membranes, the free-energy of the membrane is always smaller than that of the chain for any χ , i.e. $\bar{\mathcal{F}}_{me,\infty}^{mac} < \bar{\mathcal{F}}_{ch,\infty}^{mac}$.

The macroscopic approach is well in agreement with the experiments [8–10] which show that the formation of 3D spherical droplets is unfavorable. Namely, from Eq.(43) (further below) it is seen that for a *spherical droplet*, where $L_x = L_y = L_z = 1/3$, the free-energy is given by $\bar{\mathcal{F}}_{drop}^{mac}(\mathbf{H}_0, \hat{L}) \approx -(3/2)\mu_0 H_0^2 V \chi / (1 + \chi/3)$. This means that $\bar{\mathcal{F}}_{me,\infty}^{mac} < \bar{\mathcal{F}}_{ch,\infty}^{mac} < \bar{\mathcal{F}}_{drop}^{mac}$, i.e. also in the macroscopic approach the formation of chains and membranes (once they become large) is more favorable than the creation of spherical droplets.

B. Finite Chains and Membranes

For finite N the demagnetization factors L_i depend on the aspect ratio a/c , i.e. on N . The chain is characterized by the long semi-axis $c \sim ND$ (D the bead size), and the short semi-axis $a \sim D \ll c$, with the corresponding demagnetization factors L_a, L_b, L_c ($L_a + L_b + L_c = 1$) [15], [22–24]. The *chain-membrane transition* in the macroscopic approach is reached on the critical line $N_c(\chi)$, where $\bar{\mathcal{F}}_{me}^{mac}(N_c) = \bar{\mathcal{F}}_{ch}^{mac}(N_c)$. To demonstrate the existence of such a transition the critical line was calculated for the spheroid scheme 1 by assuming, for simplicity, that the chain and membrane material susceptibilities are the same [7]. It was found that the critical cluster size N_c grows with the material susceptibility χ . For $\chi \approx 1 - 3$, it was estimated $N_c \approx 10 - 20$. Such a tendency is also observed in experiments [10], where for $N_c \approx 10$ initial signs of the chain-membrane transition are found. In these experiments, chains are formed for small $N \sim 10$ in the very dilute limit, while a further addition of colloids results in a branching of chains (via the so called Y-junctions), further followed by a network of inter-connections and finally dense membrane patches are formed. The conclusion is that the chain-membrane

transition in the macroscopic approach is qualitatively in accord with experiments.

Let us calculate the finite N -effects in the macroscopic approach and compare it with the microscopic theory given in Section IV. To remind the reader, in the *microscopic approach* the free-energy in Section IV is calculated for small χ_b by expanding it up to χ_b^3 , i.e. it is given by $\bar{\mathcal{F}}_{cVdW}^{micro} \simeq \bar{\mathcal{F}}_{cVdW}^{(1)} + \bar{\mathcal{F}}_{cVdW}^{(3)}$ (since $\bar{\mathcal{F}}_{cVdW}^{(2)} = 0$) where $\bar{\mathcal{F}}_{cVdW}^{(1)} \propto N\chi_b$ describes N non-interacting beads, while the first nontrivial term due to the dipole-dipole interaction in Eq.(29) is $\bar{\mathcal{F}}_{cVdW}^{(3)} \propto \chi_b^3$. As already discussed, the term $\bar{\mathcal{F}}_{cVdW}^{(3)}$ is due to both, 2-body and 3-body interactions.

In order to compare these two approaches we need to expand the free-energy in the macroscopic approach as a function of χ_b up to χ_b^3 , as well. In the macroscopic approach, described by Eq.(39)-Eq.(42), the free-energy depends on the material susceptibility χ which is related to the bead susceptibility χ_b and in systems with small bead susceptibility (χ_b) χ is also small. Therefore, in order to make the expansion of the macroscopic free-energy Eq.(40) with respect to χ_b a relation between χ and χ_b is necessary. In fact χ is related to the averaged bead susceptibility $\bar{\chi}_b = \rho_{pack}\chi_b$, where $\rho_{pack}(<1)$ is the *packing (volume) fraction* of the beads in a given assembly. (Note that the total volume of the bead $V_{tot} = NV_b$ is related to the macroscopic volume V by $V_{tot} = \rho_{pack}V$.) By assuming high local symmetry around each bead within the assembled structures it is easy to show that in that case the Lorenz-Lorenz relation $\chi = \bar{\chi}_b(1 - (\bar{\chi}_b/3))^{-1}$ holds. By making an expansion of χ up to $\bar{\chi}_b^3$ and using that $L_x = L_y$ and $L_x = (1 - L_z)/2$ the *macroscopic free-energy* in Eq.(40) reads

$$\frac{\bar{\mathcal{F}}^{mac}(\mathbf{H}_0, \hat{L})}{(\mu_0 H_0^2 V/2)} \approx -3[\bar{\chi}_b + \frac{\bar{\chi}_b^3}{2}(L_z - \frac{1}{3})^2]. \quad (43)$$

Note, that in the case of the chain one has $L_z \rightarrow 0$ for $N \rightarrow \infty$, while for the membrane one has $L_z \rightarrow 1$ for $N \rightarrow \infty$ - see below.

1. Linear Chain

As mentioned before in the case of finite N the demagnetization factor $L_z(N)$ is different in the spheroid scheme 1 and the cylindrical scheme 2. Let us have a look at the difference [15, 22–24]:

(i) the *spheroid scheme 1* - In this case the chain corresponds to a prolate spheroid and the exact demagnetization factor L_z of a prolate spheroid is given in Appendix 3A Eq.(106) with $\tau_a = N$ one has $L_z \approx (\ln N)/N^2$ and the dimensionless free-energy $f_{ch,N}^{mac,1}(\equiv \bar{\mathcal{F}}_{ch,N}^{mac,1}(\mathbf{H}_0, \hat{L})/(\mu_0 H_0^2 NV_b/2))$ given by:

$$f_{ch,N}^{mac,1} \approx f_{ch,\infty}^{mac} + \rho_{pack}^2 \chi_b^3 \frac{\ln N}{N^2}, \quad (44)$$

where the energy per bead of the infinite chain is

$$f_{ch,\infty}^{mac} \approx -(3\chi_b + \frac{\rho_{pack}^2 \chi_b^3}{6}). \quad (45)$$

(ii) the *cylinder scheme 2* - In the cylinder scheme 2 a chain corresponds to a long cylinder with the aspect ratio $\tau \equiv (h/2R) \approx 2N/3 \gg 1$, h is the height (along the c -axis) and R the radius of cylinder, one has $L_z \approx 2N/\pi$ - see in Appendix 3A Eq.(109) and the corresponding free-energy $f_{ch,N}^{mac,2}(\equiv \bar{\mathcal{F}}_{ch,N}^{mac,2}(\mathbf{H}_0, \hat{L})/(\mu_0 H_0^2 NV_b/2))$ reads

$$f_{ch,N}^{mac,2} \approx f_{ch,\infty}^{mac} + \frac{2\rho_{pack}^2 \chi_b^3}{\pi N}. \quad (46)$$

By comparing Eq.(44) and Eq.(46) of the macroscopic approach with the corresponding microscopic free-energy for the finite linear chain in Eq.(31), it turns out that the linear chain is slightly better described by the long cylinder in the cylinder scheme 2.

2. Flat Membrane

(i) the *spheroid scheme 1* - In that case the flat membrane corresponds to extreme oblate spheroids with $L_z \approx 1 - \pi/2\sqrt{N}$ - see Eq.(105) in Appendix 3A and the dimensionless free-energy $f_{me,N}^{mac,1}(\equiv \bar{\mathcal{F}}_{me,N}^{mac,1}(\mathbf{H}_0, \hat{L})/(\mu_0 H_0^2 NV_b/2))$ is given by

$$f_{me,N}^{mac,1} \approx f_{me,\infty}^{mac} + \frac{\pi \rho_{pack}^2 \chi_b^3}{\sqrt{N}}, \quad (47)$$

where the free-energy per bead of the infinite flat membrane is

$$f_{me,\infty}^{mac} \approx -(3\chi_b + \frac{2\rho_{pack}^2 \chi_b^3}{3}). \quad (48)$$

(ii) the *cylinder scheme 2* - In this case a thin cylinder with aspect ratio $\tau \approx 1/\sqrt{N} \ll 1$, one has $L_z \approx 1 - \ln N/\pi\sqrt{N}$ which gives the dimensionless free-energy $f_{me,N}^{mac,2}(\equiv \bar{\mathcal{F}}_{me,N}^{mac,2}(\mathbf{H}_0, \hat{L})/(\mu_0 H_0^2 NV_b/2))$

$$f_{me,N}^{mac,2} \approx f_{me,\infty}^{mac} + \rho_{pack}^2 \chi_b^3 \frac{\ln N}{\sqrt{N}} \quad (49)$$

By comparison with the microscopic energy in Eq.(35) one expects that the cylinder scheme 2 mimics the membrane better than the spheroid scheme 1.

C. Spherical Shell Membrane

In the microscopic approach we calculated the energy of a closed, monolayered spherical membrane (spherical shell) under the action of cVdW interaction. It is interesting to study its energetics in the macroscopic approach

where the outer and inner radius of the spherical shell are R_o , R_i , respectively, while the relative magnetic permeability in the shell is $\mu_{shell} = 1 + \chi$. Outside this shell we assume $\mu_{out} = 1$. In this case the symmetry implies that Eq.(40) is simplified to

$$\bar{\mathcal{F}}_{cVdW,shell}^{mac}(\mathbf{H}_0, \hat{L}) = -\frac{3}{2}\mu_0 H_0^2 \alpha_{shell}, \quad (50)$$

where $\alpha_{shell} \equiv V\chi_{shell}$ can be calculated in the magnetostatic limit by using standard boundary conditions [16]

$$\alpha_{shell} = 4\pi R_o^3 \frac{\chi(3+2\chi)(1-\phi)}{(\chi+3)(3+2\chi)-2\phi\chi^2}. \quad (51)$$

with $\phi = (R_i/R_o)^3$ where R_i is the inner and R_o is the outer radius of the spherical shell. For a small shell thickness $D \ll R_o, R_i$ one has $R_o^3 - R_i^3 \approx N(D/2)^3$. For the outer surface with $4\pi R_o^2 \approx \pi N(D/2)^2$ one has $\phi = 1 - N(D/2R_o)^3 = 1 - 8/\sqrt{N}$. For a small bead susceptibility $\chi_b < 1$ the material susceptibility is given by $\chi \approx \tilde{\chi}_b(1 + (\tilde{\chi}_b^2/3) + (\tilde{\chi}_b^3/9))$. By making an expansion for large N it is straightforward to obtain α_{shell} and $\bar{\mathcal{F}}_{shell}^{mac}$ in Eq.(50)

$$f_{shell,\infty}^{mac} = f_{me,\infty}^{mac} + \frac{16}{3} \frac{\varrho_{pack}^2 \chi_b^3}{\sqrt{N}}. \quad (52)$$

The first term characterizes the infinite flat membrane, while the second one $\propto (16\varrho_{pack}^2 \chi_b^3/3)N^{-1/2}$ is asymptotically smaller than that for the flat membrane $\propto (\varrho_{pack}^2 \chi_b^3)N^{-1/2} \ln N$ in Eq.(43). This means that the free-energy of the spherical membrane (with some large but finite N) becomes overall smaller than the microscopic free-energy of the finite flat membrane. This confirms our previous analysis that a large spherical membrane is slightly more favorable than the flat one.

D. Consistency of Microscopic and Macroscopic cVdW Theory

Let us check if the macro- and microscopic theory agree in concrete cases. For that purpose we compare the corresponding interacting parts of the free-energy, i.e. $\Delta f_{\infty}^{mac} (= f_{\infty}^{mac} - \frac{3}{2}\chi_b)$ and Δf_{∞}^{mic} , for chains and membranes. In the case of the chain one has $V = \rho_{pack}V_0$ and $\Delta f_{ch,\infty}^{mac} \approx -\chi_b^3 \rho_{pack}^2/6$, while the first term of the microscopic free-energy in Eq.(31) is $\Delta f_{ch,\infty}^{mic} \approx -\zeta^2(3)\chi_b^3 H_0^2/24$. The equality $\Delta f_{ch,\infty}^{mac} = \Delta f_{ch,\infty}^{mic}$ gives the consistency condition for the bead packing fraction $\rho_{pack} = 0.5\zeta(3) \approx 0.6$ - indeed a rather plausible and realistic value for the packing density. A similar situation holds for membranes, where Eq.(43) gives $\Delta f_{me,\infty}^{mic} \approx -2\chi_b^3 \rho_{pack}^2/3$. The microscopic free-energy of the flat membrane can be obtained, for instance, from Eq.(38) for the tubular membrane in the limit $R_{\perp} \rightarrow \infty$, i.e. $\Delta f_{me,\infty}^{mic} = -(\pi^4/162)\chi_b^3$. The

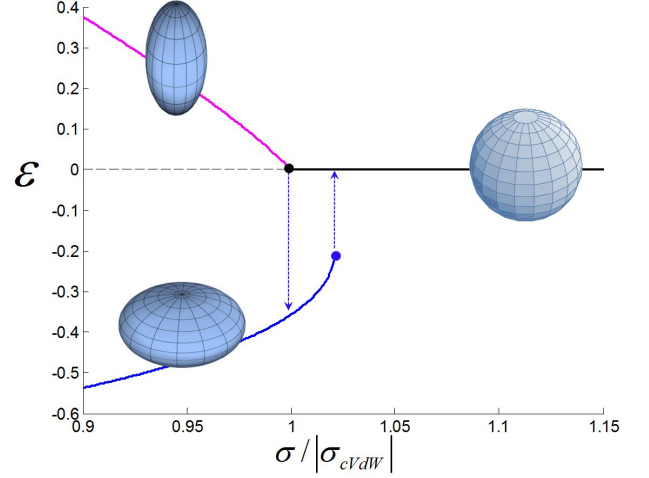


FIG. 6: cVdW induces buckling of a fluid droplet as function of the scaled surface tension. ε is the eccentricity of the ellipsoid with $\varepsilon < 0$ - oblate ellipsoid; $\varepsilon > 0$ - prolate ellipsoid

condition $\Delta f_{me,\infty}^{mac} = \Delta f_{me,\infty}^{mic}$ gives the packing fraction $\rho_{pack} \approx 0.9$ which is a reasonable value.

The good news overall is, that for several types of assemblies we confirm a qualitative and a satisfactory quantitative agreement of the macroscopic approach with the microscopic one in cases considered. This justifies the more coarse grained but simpler macroscopic approach in studying several cVdW structures.

E. Instability of The Spherical Droplet

We have seen that the many body interactions in cVdW systems favor the formation of large membrane structures. The latter behavior could be interpreted as coming from an effective negative "surface tension". It appears that cVdW tends to "flatten out" every aggregate into a thin monolayered sheet down to the smallest cut-off length (the constituent bead size)- as if a negative effective surface tension was at work.

In this *Section* we show on a concrete example that the cVdW assemblies indeed behave as systems with negative effective surface tension $\sigma_{cVdW} < 0$. Although this quasi-surface tension is in reality a rather complex and anisotropic *bulk* term (and depends on the shape of assemblies) it generates effects which are very reminiscent of a real surface tension.

To crystallize out the physics, in the following we will let the cVdW interaction directly compete with an additional real (positive) fluid surface tension. Concretely, we consider a cVdW system made of paramagnetic beads which are embedded in a spherical droplet of the solvent, say oil or water, with the surface tension σ . Now, the question is : What is the critical surface tension below which the spherical droplet becomes unstable and starts forming an oblate ($\tau_s < 1$) or prolate ($\tau_s > 1$) spheroid?

Here $\tau_s = c/a$ is the aspect ratio of the spheroid.

For shapes very close to the sphere, one can expand the total free-energy in terms of the small z -axial stretch $\varepsilon = \tau_s - 1 \ll 1$, where $\varepsilon < 0$ represents an oblate ellipsoid and $\varepsilon > 0$ means a prolate one. By using Eq.(104) given in *Appendix 3B* one obtains the z -axis demagnetization factor L_z . The results for L_z holds in both cases the oblate spheroid and prolate one, and we furthermore have $L_x = L_y = (1 - L_z)/2$. By using the latter property the dimensionless free-energy in Eq.(43) takes the form

$$\frac{\bar{\mathcal{F}}_{cVdW} - \bar{\mathcal{F}}_0}{E_0} = - \left(\frac{8}{75}\varepsilon^2 - \frac{24}{175}\varepsilon^3 + \frac{1382}{11025}\varepsilon^4 \right) + O(\varepsilon^5),$$

with $E_0 = \mu_0 \tilde{\chi}_b^3 V H_0^2 / 2$ the convenient energy scale and $\bar{\mathcal{F}}_0$ the non-interacting (self-) free-energy of all beads.

Introducing also the surface energy term σA to the total energy we have then

$$\bar{\mathcal{F}}_{tot} = \bar{\mathcal{F}}_{cVdW} + \sigma A \quad (53)$$

where the surface area of spheroid A depends on the aspect ratio τ_s and is given in *Appendix 3B*. A short calculation then gives

$$\begin{aligned} \frac{\bar{\mathcal{F}}_{tot}}{E_0} = & - \left(\frac{8}{75}\varepsilon^2 - \frac{24}{175}\varepsilon^3 + \frac{1382}{11025}\varepsilon^4 \right) \\ & + \frac{\sigma A_0}{E_0} \left(\frac{8}{45}\varepsilon^2 - \frac{584}{2835}\varepsilon^3 + \frac{118}{567}\varepsilon^4 \right). \end{aligned} \quad (54)$$

We see that the sphere with radius R is only stable when the ε^2 term is positive which implies

$$\begin{aligned} \frac{\sigma A_0}{E_0} & > \frac{3}{5} \equiv \frac{\sigma_{cr} A_0}{E_0} \\ \sigma_{crit} & = \frac{1}{5} \mu_0 \tilde{\chi}_b^3 H^2 R, \end{aligned} \quad (55)$$

where $\mu_0 \tilde{\chi}_b^3 H^2 R / 5$ may be considered as an effective cVdW surface tension σ_{cVdW} , which has however a negative sign and counteracts (reduces) the actual surface tension of the surrounding liquid.

The phase diagram for the cVdW spherical droplet is shown in Fig.6. Notably for a subcritical fluid surface tension $\sigma < \sigma_{crit}$ the droplet can be either prolate or oblate. Which branch is actually chosen might subtly depend on the dynamics and history of the shape. However, from energetic point of view, the absolute energy minimum in the subcritical regime is reached for the flatter i.e. oblate shape (lower ε stable branch). The elongated prolate ellipsoid forms only a shallow local minimum and is therefore thermodynamically only metastable.

The effective surface tension $\sigma_{cVdW}(R)$ is in reality a many-body bulk term and thus size dependent. Let us estimate on which scale it becomes relevant, for instance, in a drop of water, with surface tension $\sigma_{H_2O} = 0.073 \text{ J/m}^2$ (at room temperature). For $\chi_b \sim 1$ and

$B = \mu_0 H_0 = 0.01T$, the cVdW surface tension is $\sigma_{crit} \approx -B^2 R / 5 \mu_0 = -15.9 (J/m^3) R$. For this to be of the same order as σ_{H_2O} we need the radius of the droplet to be $R_c = 5 \sigma_{H_2O} / (\mu_0 \chi_b^3 H^2) = 4.6 \times 10^{-3} \text{ m} = 4 \text{ mm}$. For larger droplets made of paramagnetic beads with $R > R_c$ the spherical shape becomes unstable.

In the dielectric analogue of this phenomenon in cVdW systems we would have $\sigma_{crit} = \varepsilon_0 \kappa_{el}^3 E^2 R / 5$. Let us assume that the dielectric droplet has much smaller dielectric susceptibility than of the electric beads ($\kappa_{el,m} \ll \kappa_{el}$) and that the surface tension is of the order as that of water. Then for a feasible electric field $E = 10 \text{ V/mm}$, $\varepsilon_0 = 8.8 \times 10^{-12} \text{ J/mV}^2$, and for $\kappa_{el}^3 \sim 1$ we have $R_{el} = 5 \sigma / (\varepsilon_0 \kappa_{el}^3 E^2) \approx 500 \text{ m}$! This means that this effect is less favorable in the electric case. However, for magnetic colloids (such as ferrofluids) under magnetically induced cVdW, the "negative surface tension" instability effect should be easily observable.

VI. FORMATION OF SUPERSTRUCTURES IN CVDW SYSTEMS

In magnetically driven cVdW systems chains and membranes are the predominant structures formed on intermediate length and timescales [8–10]. However, the experiments also show that in more dense colloid systems which are placed in containers of finite volume, more complex structures like foams are formed on larger scales. The existence of these foam structures is also confirmed in numerical simulations [8, 9]. The basic motif underlying such foams, is a complex network of interconnected membrane patches, which apart from touching along their edges do not stack and aggregate. Instead the membranes seem, at least by visual inspection, to repel each other and the whole foam structure appears to swell against gravity. What is the origin of such large scale cVdW foam structures?

In this Section we give a plausible physical explanation by combining both the microscopic and macroscopic approaches. First, we will study the cVdW interaction free-energy of two flat membranes. We show below that this interaction switches from an attraction to a repulsion, depending on the mutual orientation.

While in general, the interactions between two membranes can have both signs, it turns out that in the majority of possible configurations the interaction is in fact repulsive on the average. Then, we calculate the free-energy of the foam structure by modelling it by a cubic shelf structure ansatz. We show that such a structure indeed tends to swell and at the end we derive something that reassembles an equation of state of a cVdW foam, i.e. a pressure-concentration-field relation. We show that the magnitude of this pressure is quite notable and can indeed lead to a rise of the foam to measurable heights.

A. cVdW Interaction Generalization to Anisotropic Objects

In the previous sections we were concerned with interactions of isotropic spherical particles whose susceptibility tensors were merely diagonal $(\hat{\chi}_b)_{\alpha\beta} = \chi_b \delta_{\alpha\beta}$ i.e. simply a number. Here we generalize the interaction to any two arbitrary shaped bodies. In general this is a complicated problem when the bodies are very close. However, when they are far enough, say much further than their typical body extensions, the field of any object can be replaced with a corresponding effective ellipsoid field. In this sense it is sufficient to consider the interaction of two ellipsoids, with orientation dependent and non-trivial susceptibility tensors $\hat{\chi}_1, \hat{\chi}_2$. The free-energy in this case can be rewritten in the form

$$\bar{\mathcal{F}}_{cVdW}(\mathbf{H}_0, \{\mathbf{R}_i\}) = -\frac{\mu_0 H_0^2}{2} \text{Tr}(V_1 \hat{\chi}_{1,eff} + V_2 \hat{\chi}_{2,eff}), \quad (56)$$

where $\hat{\chi}_{1,eff}$ and $\hat{\chi}_{2,eff}$ are now effective susceptibility tensors of the two bodies (ellipsoids) with respective volumes $V_{1/2}$. The effective susceptibility tensors are now given by the expression

$$\hat{\chi}_{1,eff} = (1 - \varphi_{12}^2 \hat{\chi}_1 \hat{t}_{12} \hat{\chi}_2 \hat{t}_{12})^{-1} (\hat{\chi}_1 - \varphi_{12} \hat{\chi}_1 \hat{t}_{12} \hat{\chi}_2) \quad (57)$$

and same for the second $\hat{\chi}_{2,eff}$ which is obtained by replacing $1 \rightarrow 2$. The slightly more intricate form of $\hat{\chi}_{1/2,eff}$, which is obviously a generalization of the corresponding isotropic expression Eq.(9), comes now from the fact that the operator $\hat{t}_{12} = \hat{1} - 3|\mathbf{b}_{12}\rangle\langle\mathbf{b}_{12}|$ and the susceptibilities $\hat{\chi}_i$ are operators with spacial orientations which don't commute now any more in general.

The expressions in Eq.(56 -57) are general and contain the distance dependence through the scalar factor $\varphi_{12} \propto 1/|\mathbf{R}_{12}|^3$ in a slightly scrambled form that hides the leading order scaling. Thus, it is interesting to expand $\hat{\chi}_{1/2,eff}$ to the first order w.r.t. φ_{12} and obtain the leading order interaction part

$$\bar{\mathcal{F}}_{cVdW,inter}(1,2) = \frac{\mu_0}{2} H_0^2 V \varphi_{12} \text{Tr}\{(\hat{\chi}_1 \hat{\chi}_2 + \hat{\chi}_2 \hat{\chi}_1) \hat{t}_{12}\}. \quad (58)$$

Here we omit trivial self-energies, i.e. consider the interaction energy term only, and assume the two bodies to have the same volume V . Note that, when the objects are isotropic (e.g. spheres, point like) then the $\hat{\chi}_{1/2}$ turn simply into numbers. Reminding ourselves that \hat{t}_{12} is traceless we see that the whole term $\propto \varphi_{12}$ vanishes in the isotropic case. This is why the cVdW interaction for two spheres only starts out with a higher order leading $\propto \varphi_{12}^2 \propto 1/|\mathbf{R}_{12}|^6$ interaction term. However in general, for anisotropic objects the trace in Eq.(58) is non-zero, giving rise to a strong and long range interaction $\propto 1/R^3$. That is, anisotropic objects interact much stronger than isotropic ones under cVdW. Once growing aggregates become shape anisotropic and notably they always tend to do so (forming chains and membranes), they interact in

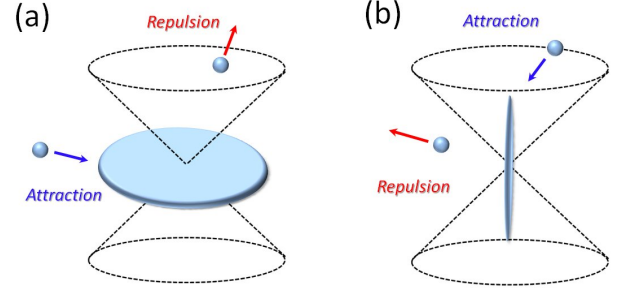


FIG. 7: The cVdW interaction for a bead interacting with (a) an oblate membrane (cf. Eq.(59)) and (b) a prolate chain.

a long range manner. This can be seen as another manifestation of the cooperative many-body nature of cVdW.

B. Interaction of Membrane and Single Spherical Bead

To understand the content of the anisotropic cVdW interaction from Eq.(58), let us have a look at how a flat membrane interacts with a single spherical bead. The effects of beads approaching chains and membranes were previously studied numerically by Osterman et al. [10]. Interestingly, it turns out, that even in this simplest case the interaction can vary in sign. It is attractive when the membrane is approached by the bead from the edge side. When however approaching from the top, in the direction of the membrane normal, the bead is repelled in the far field. If the bead approaches the membrane even further (against the repulsive force) and comes closer in this normal direction, the interaction switches again to a short range attraction. Obviously there is a barrier to cross in this normal direction. The largest barrier for joining of the bead to the membrane is when the former is above the center of the membrane and we study this case first - see Fig.(7a). By applying Eq.(14) on two particles, where the first one is big and anisotropic - it mimics a membrane, while the second one is small and isotropic - it mimics a bead, one obtains the free-energy in the form

$$W^{m-b} = -\frac{1}{2} \mu_0 H_0^2 V_0 (q_m \text{Tr} \hat{\chi}_{m,eff} + q_b \text{Tr} \hat{\chi}_{b,eff}) \quad (59)$$

$$= W^m + W^b \quad (60)$$

Here, $V_0 = V_m + V_b$, $q_{m,b} = V_{m,b}/V_0$ and V_m, V_b is the volume of the membrane and bead, respectively, while $\hat{\chi}_{m,eff}$ and $\hat{\chi}_{b,eff}$ the effective susceptibilities of membrane and bead respectively with

$$\hat{\chi}_{m,eff} = \frac{1}{(1 - q_m q_b \varphi_0^2 \hat{\chi}_m \hat{t} \hat{\chi}_b \hat{t})} \hat{\chi}_m (1 - q_m \varphi_0 \hat{t} \hat{\chi}_b). \quad (61)$$

and $\hat{\chi}_{b,eff}$ is obtained by replacing $m \leftrightarrow b$ in Eq.(61) and $\varphi_0 = V_0/4\pi R_{mb}^3$. In this approach the membrane

is replaced by an oblate spheroid with the susceptibility $\hat{\chi}_m = \chi_{\min} |\mathbf{n}_m\rangle \langle \mathbf{n}_m| + \chi_{\max} (1 - |\mathbf{n}_m\rangle \langle \mathbf{n}_m|)$, while for the spherical bead we have $\hat{\chi}_b = \chi_b \hat{1}$; \mathbf{n}_m is the unit vector normal to the membrane. The tensor \hat{t} in Eq.(61) is $\hat{t}(\equiv \hat{t}_{m-b}) = \hat{1} - 3 |\mathbf{b}_{m-b}\rangle \langle \mathbf{b}_{m-b}|$. Since we assume that the membrane's dimensions are much larger than the bead size D and the bead is above the membrane one has $\mathbf{n}_m \parallel \mathbf{b}_{m-b}$, i.e. $\hat{t}_{m-b} = 1 - 3 |\mathbf{n}_m\rangle \langle \mathbf{n}_m|$.

The final expression for the dimensionless free-energy $w^{m-b} = W^{m-b}/(\frac{1}{2}\mu_0 H_0^2 V_0) = w^m + w^b$ is given by (cf. *Appendix 4A*)

$$w^m = -\frac{q_m \chi_{\max}}{1-b} \left\{ 2(1-\alpha_b) + \frac{\chi_{\min}}{\chi_{\max}} \frac{1+2\alpha_b}{1+c} \right\} \quad (62)$$

$$w^b = -\frac{q_b \chi_{\max}}{1-\alpha_m \alpha_b} \left\{ \frac{3+2c}{1+c} + 2 \frac{\chi_{\min}}{\chi_{\max}} \frac{\alpha_m}{1+c} - 2\alpha_m \right\}, \quad (63)$$

where $\alpha_b = q_b \chi_b \psi_0$, $\alpha_m = q_m \chi_{\max} \psi_0$; $c = (\alpha_m \alpha_b (\chi_{\max} - 4\chi_{\min}))/\chi_{\max} (1 - \alpha_m \alpha_b)$. Let us discuss the energy of the membrane-bead complex as a function of their distance $r = R_{m-b}/D$ by assuming (for simplicity) that $\chi_{\min} \ll \chi_{\max}$ i.e. a very flat membrane. Since $q_b \ll q_m \simeq 1$ one has $\alpha_m \alpha_b \ll 1$ and the expression simplifies to

$$\frac{w^{m-b}}{2\chi_{\max}} \simeq -1 + \frac{\chi_b}{24} \left(\frac{2}{r^3} - \frac{\chi_{\max}}{24q_b} \frac{1}{r^6} \right). \quad (64)$$

From Eq.(64) we see that there is an energy barrier for the bead, i.e. for $R_{m-b} > R_c = D(\chi_{\max}/24q_b)^{1/3}$ the membrane repels the bead since $F_{m-b} = -(\partial W^{m-b}/\partial R_{m-b}) > 0$, while for $R_{m-b} < R_c$ the force is attractive ($F_{m-b} < 0$). As an example we take $\chi_{\max} \sim 10$ and $q_b > 10^{-3}$ which gives us the barrier at a notable distance $R_c > 10D$ - larger than the bead size. Based on the same formalism it is straightforward to show that when the bead is placed in the plane containing the membrane, i.e. when $\mathbf{n}_m \perp \mathbf{b}_{m-b}$ holds, it is always attracted to the membrane, i.e. $F_{m-b} < 0$.

To conclude, the above considerations show that the most favorable and fastest membrane growth pathway is addition of beads along the membrane edges in membrane's plane. Those beads found above the membrane must move parallel to the membrane and finally descend toward the ends of membranes. This is schematically shown in Fig.7a for a bead interacting with a membrane and in a Fig.7b for a bead interacting with a chain (prolate ellipsoid). In the latter case calculations go along the same lines as for membranes, with the only difference being in flipping the signs of interaction. The beads are repelled laterally and attracted along the symmetry axis of the chains. The easy calculation being very similar as for membranes is omitted here.

C. Interaction of Two Membranes

Once they emerge, what is the fate of the membranes as they continue growing? At some point the mem-

branes will run out of free beads in the solution and start interacting only with the remaining aggregates which turn into membranes once they are large enough. To understand, how two membranes mutually order, we need the *2-membrane interaction* for arbitrary membrane orientations $\mathbf{n}_{1,2}$ and anisotropic susceptibilities $\hat{\chi}_i^{(L)} = \chi(1 + \hat{L}_i \chi)^{-1}$. For identical membranes and at large distances ($\varphi_{12} \ll 1$, i.e. for $|\mathbf{R}_{12}| \gg V_m^{1/3}$) one expands $\hat{\chi}_{eff,12} \approx \hat{\chi}_1^{(L)} (1 - \varphi_{12} \hat{t}(\mathbf{b}_{12}) \hat{\chi}_2^{(L)})$ and the long range interaction energy in Eq.(9) after a short calculation reads (see details in *Appendix 4B*),

$$\frac{\bar{\mathcal{F}}_{int}}{\alpha} = \frac{C_1^2 + C_2^2 + \frac{1-\gamma}{3} C_3^2 - (1-\gamma) C_1 C_2 C_3 - \frac{2}{3}}{|\mathbf{R}_{12}|^3} \quad (65)$$

with $\alpha = 3(1-\gamma)\chi_{\max}^2 \mu_0 H_0^2 V_m^2 / 16\pi$, and $\gamma = \chi_{\min}/\chi_{\max}$ the ratio of the minimal/maximal eigenvalue of the membrane susceptibility tensor $\hat{\chi}^{(L)}$.

The dimensionless factors $C_1 = \mathbf{n}_1 \cdot \mathbf{b}_{12}$, $C_2 = \mathbf{n}_2 \cdot \mathbf{b}_{12}$, $C_3 = \mathbf{n}_1 \cdot \mathbf{n}_2$ reveal all the geometrical beauty of cVdW: the 2-membrane interaction is angle dependent and repulsive in many configurations - see Fig.8. Notably, for a fixed $|\mathbf{R}_{12}|$, $\bar{\mathcal{F}}_{int}$ becomes minimal for the orthogonally *twisted* membrane orientation with $\mathbf{n}_1 \perp \mathbf{n}_2$, $\mathbf{n}_1 \perp \mathbf{b}_{12}$ and $\mathbf{n}_2 \perp \mathbf{b}_{12}$ ($C_{1/2/3} = 0$). The twisted membranes attract each other since $\bar{\mathcal{F}}_{int}^{(tw)} < 0$ (up to the point of mutual contact), as in the *coplanar* case, yet the *twisted* configuration has lower energy. This interesting result should affect the kinetics of membrane formation: If two distant membranes start growing within a large distance they will rotate to a 90° position before touching. Therefore, some type of glassy state in their orientation may be kinetically favored. In other relevant configurations, such as the *top*, with two out of plane parallel membranes ($C_{1/2/3} = 1$) or the *generic* one (cf. Fig.8), the interaction is repulsive with $0 < \bar{\mathcal{F}}_{int}^{(gen)} < \bar{\mathcal{F}}_{int}^{(top)}$.

D. Emergence of Foams

Simulations and experiments [8, 9] provide some empirical evidence for the existence of a hollow foam-like superstructure forming on large scales (cf. Fig 9a). What is the physical mechanism driving such a cVdW foam formation?

We have seen above that large aggregates prefer to form membranes, and that these membranes mutually interact. Specifically, when two distant membranes are stacked over each other they repel each other ($\bar{\mathcal{F}}_{int}^{(top)} > 0$). In the opposite limit - in close contact distance- a simple estimate implies their preference to split as well. Namely, when a thick membrane, with the thickness $2D$, radius R and volume $2V_m$, is cut into two parallel membranes, with the thickness D and radius R each and separated to infinite distance there is a gain in the energy $\Delta\mathcal{F} = 2\mathcal{F}_{1m} - \mathcal{F}_{2m} \approx -V_{2m} L \chi^2 (1 - (1 + \chi)^{-2}) < 0$ for

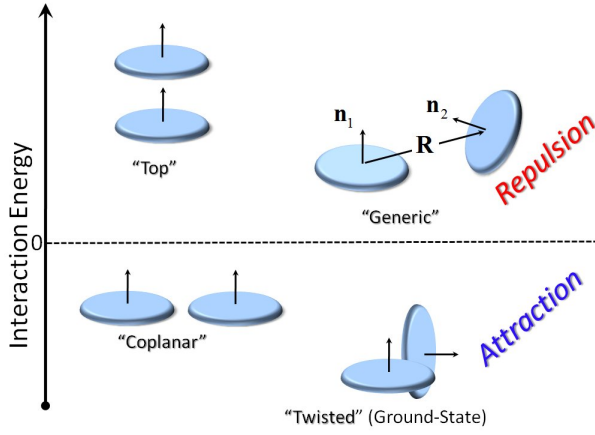


FIG. 8: The cVdW for two interacting membranes is unexpectedly complex. The 2-membrane interaction is attractive or repulsive depending on orientation, cf. Eq.65 with a ground state in the "twisted" configuration.

$L\chi \ll 1$, where $L \propto D^{3/2}V_{2m}^{-1/2}$. Physically this means that the second membrane lying above the first one is repelled to increase the local fields with respect to the thicker membrane case.

It is this remarkable reluctance of membranes to mutually stack that in fact sets the microscopic structure of the foam: It is formed out of the thinnest possible membrane patches, whose thickness is collapsed onto the smallest available physical scale - the bead size D . The characteristic lateral size a_M of these membrane patches, on the other hand, is set by the bead volume fraction in the container $f_V = V_b^{tot}/V \ll 1$ (with $V_b^{tot} = NV_b$ the total volume of all beads and V the container's volume). By assuming a cubic shelf structure as an ansatz, cf. Fig 9b, one obtains a patch size $a_M \approx 3D/f_V$.

In order to calculate the pressure in such a foam structure we need the total interaction free-energy of all membranes in the system. It turns out that the interaction part of the free-energy ($\bar{\mathcal{F}}_{int}$) of the assumed cubic shelf structure is positive ($\bar{\mathcal{F}}_{int} > 0$) due to global average repulsion of membranes - see *Appendix 4C*.

VII. EQUATION OF STATE OF CVDW FOAMS

In the previous Section we have argued qualitatively that in the cVdW foam structure the positive interaction free-energy should favor an effective repulsion between constituent membranes forming this structure, i.e. that the foam should exert a pressure on walls of the container and in fact swell. In this Section we calculate this pressure as a function of the volume fraction of magnetic beads, i.e. we derive the equation of state for a cVdW material.

As above we define the volume fraction of all beads in the container $f_V = (N_m V_m / V) \approx V_b^{tot} / V$ where $V_m (\approx$

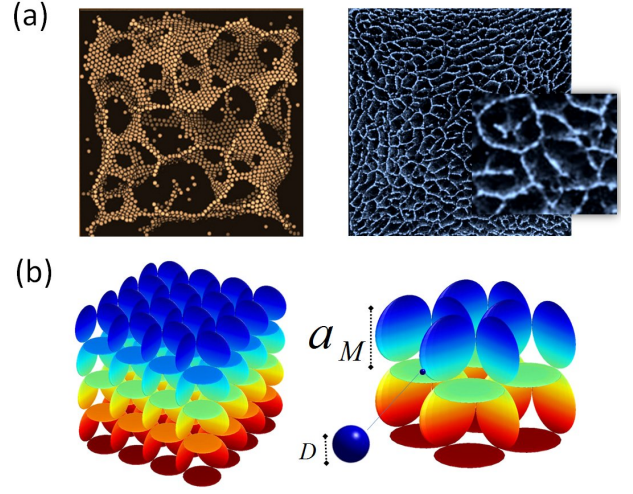


FIG. 9: (a) The large scale structure of a dipolar cVdW foam (from [8, 9]) in experiment (right) and in simulation (left). (b) The theoretical 3D shelf-model for cVdW foam's structure.

Da_M^2) is the volume of the single membrane and N_m is the total number of (equal) membranes in the container volume $V \approx Na_M^3$, and V_b^{tot} is the total volume of the beads. Here, D is the bead diameter and a_M is the size of the single membrane - see Fig.9b. It follows that $f_V \approx 3D/a_M$.

In the following we fix the total volume of all N_m membranes $V_m^{tot} = N_m V_m$ and vary the size of the container V . The pressure is then defined by $p = -\partial \bar{\mathcal{F}}^{tot} / \partial V$ where $\bar{\mathcal{F}}^{tot} = \bar{\mathcal{F}}_{self}^{tot} + \bar{\mathcal{F}}_{int}^{tot}$ is the total energy of the membranes. $\bar{\mathcal{F}}_{self}^{tot}$ is the self-energy of (non-interacting) membranes and $\bar{\mathcal{F}}_{int}^{tot}$ is the interaction energy of membranes. From Eq.(40) the free-energy of the N_m single membranes (the self-energy) with the total volume $V_m^{tot} = N_m V_m$ is given by

$$\bar{\mathcal{F}}_{self}^{tot} = -(2\chi_{\max} + \chi_{\min})V_m^{tot} \frac{B_0^2}{2\mu_0}, \quad (66)$$

$$\chi_{\max} = \frac{\chi}{1 + L_m \chi}, \quad \chi_{\min} = \frac{\chi}{1 + (1 - 2L_m)\chi}. \quad (67)$$

For simplicity, we study here only the case with large material susceptibility $\chi > 1$ (note that, the material susceptibility fulfills $\chi > \chi_b \leq 3$, where χ_b is the bead susceptibility with respect to the applied (external) field) and at the same time $L_m \chi \ll 1$ ($L_m \ll 1$).

In the following we approximate, for simplicity, the membranes by oblate spheroids. The demagnetization factor of the flat membranes in the plane direction can be related with the membrane aspect ratio, which itself is set by the volume fraction $L_m \approx f_V/4$ (for $f_V \ll 1$). After a straightforward expansion with respect to small L_m one obtains

$$\bar{\mathcal{F}}_{self}^{tot}(V) \approx -(Const - \frac{1}{2}f_V \chi^2)V_m^{tot} \frac{B_0^2}{2\mu_0}, \quad (68)$$

where $Const$ is independent of the volume fraction f_V .

The *total interaction energy* of membranes $\bar{\mathcal{F}}_{int}^{tot}$ is on the other hand

$$\bar{\mathcal{F}}_{int}^{tot}(V) = \frac{1}{2} \sum_{i,j} \bar{\mathcal{F}}_{int}(i,j), \quad (69)$$

where the pair-interaction energy $\bar{\mathcal{F}}_{int}(i,j)$ is given by Eq.(65) where the summation goes over all membranes in the container. Note, that for the nearest neighbor membranes with $|\mathbf{R}_{12}| \approx a_M$ the far field approximation Eq.(65) holds qualitatively only, while for the next-nearest neighbors it holds already quantitatively. For $\chi \gg 1$ and $L_m \chi \ll 1$ Eq.(69) gives

$$\bar{\mathcal{F}}_{int}^{tot}(V) \approx \left(\frac{1}{8\pi} f_V \chi^2 S\right) V_m^{tot} \frac{B_0^2}{2\mu_0}, \quad (70)$$

where the explicit expression for the sum $S(= a_M^3 \bar{\mathcal{F}}_{int}/\alpha) \approx 10$ - a numeric dimensionless constant - is calculated by explicitly summing over all the pairwise membrane-membrane interactions (given by Eq.(65)) in the cubic shelf lattice, for details cf. *Appendix 4C*.

Finally, combining both contributions to the free energy (self-energy and total interactions), the total pressure of the foam in a container with the volume V is given by

$$p = -\frac{\partial \bar{\mathcal{F}}^{tot}}{\partial V} \approx \left(\frac{1}{2} + \frac{S}{8\pi}\right) \chi^2 f_V^2 \left(\frac{B_0^2}{2\mu_0}\right). \quad (71)$$

As a result the foam's pressure is given by the approximate expression

$$p \approx \frac{1}{2} \mu_0 \chi^2 f_V^2 H_0^2. \quad (72)$$

Interestingly, this pressure can assume notable magnitudes in practice. For moderate volume fractions, reasonable fields and susceptibilities ($f_V \approx 5 \cdot 10^{-2}$, $\mu_0 H_0 \approx 20mT$, and $\chi \approx 10$ in densely packed *Ni*-beads membranes) we obtain $p \approx 40 Pa$. Since $p \propto H_0^2$, the pressure is very sensitive to the strength of the excitation (field) H_0 and can lead to strong swelling of the foam against gravity. The latter effect is also observed experimentally [25] and can be used to practically test the equation of state Eq.(72).

A. Gravitational Pressure of the Foam

Since a real foam is formed in the gravitation field, the gravity can limit its swelling. As we see from Eq.(72) the foam's pressure p is proportional to f_V^2 and in the gravitational field both are dependent on the vertical height position h along the gravity direction. If one assumes that at $h = 0$ the volume fraction takes the value $f_{V,0}$ and the pressure p_0 then (in case of constant f_V and p) the foam would grow up to the maximal height

$h_{max}^0 = p_0 / \Delta \rho g f_{V,0}$, where $g \simeq 10m/s^2$, is the gravitational acceleration and $\Delta \rho = \rho_{bead} - \rho_s$ is the difference in densities of magnetic beads and solvent. For instance, for water immersed *Ni*-beads as in Refs. [8, 9] one has $\Delta \rho \simeq 8 \cdot 10^3 kg/m^3$. For $f_{V,0} \approx 5 \cdot 10^{-2}$, $\mu_0 H_0 \approx 20mT$, and $\chi \approx 10$ in densely packed *Ni*-beads membranes one obtains the pressure $p^{(1)} \approx 40 Pa$ and the equilibrium foam height h is reached once the internal and the gravitational pressure balance, i.e. $p \approx \Delta \rho g f_{V,0} h_{max}^0$ and the foam will swell strongly up to $h_{max}^0 \sim 1 cm$.

The variation of pressure $p(h)$ and the volume fraction $f_V(h)$ with the height in the gravitational field changes this approximative analysis slightly. In the gravitational field one has

$$\frac{dp}{dh} = -\Delta \rho g f_V. \quad (73)$$

By using the equation of state in Eq.(72) - with $f_V = C \cdot \sqrt{p}$, the solution of Eq.(73) reads

$$p(h) = p_0 \left(1 - \frac{h}{2h_{max}}\right) \quad (74)$$

$$f_V(h) = f_{V,0} \left(1 - \frac{h}{2h_{max}}\right).$$

The maximal height is reached when $p = 0$, i.e. when $h_{max}^{(1)} = 2h_{max}^0$. For the above parameters one obtains $h_{max}^{(1)} \sim 2 cm$.

Therefore, the strong swelling behavior of magnetic foams can be used as a sensitive test of the theory.

VIII. SUMMARY AND DISCUSSION

We have studied the formation of hierarchical superstructures in systems driven by the spatially coherent Van der Waals (cVdW) interaction. We have developed a fairly general formalism involving the effective susceptibility tensor which allowed us to walk through all the important aspects of the cVdW interaction. Within this setting, in a bottom up approach we investigated numerous phenomena, from dimer formation, over 3 body forces, then collective elasticity of intermediate structures (chains and membranes) up to the presumably highest scale of pattern formation, i.e. to the cVdW foams.

In the theory we took a bird's view approach, and we have shown that the cVdW interaction can be equivalently created in many types of excitation fields, generalizing the triaxial balanced fields used in the past. It turned out that the consideration of a general square isotropic uniform field (rather than any particular realization of it), brings the cVdW and its classical incoherent VdW "sister"-interaction onto a common footing. This parallel consideration of cVdW- and VdW-matter allowed us also to crystallize out the common behavior, but more importantly the central differences between the two types of forces behind them.

The most remarkable difference is found in the 3-body interactions. For the standard VdW matter the 3-body forces are recovered in the fully incoherent limit of our formalism and they agree with the classic result of Axilrod and Teller [18]. These VdW 3-body forces are much weaker and shorter ranged than the corresponding 2-body forces, i.e. one could say they are *subdominant* and give only higher order corrections. In sharp contrast, in the cVdW-matter the 3-body forces derived here are as strong and often even stronger than the pairwise 2-body ones. Thus, the 3-body effects under the cVdW interaction can be considered as *essential* and *dominant* forces in the system. To our knowledge, this "many body dominance" makes the cVdW force stand out among other known interactions and gives it a very unique, interesting character. We have studied the physical origin of these dominant cVdW many body forces and we found them originating from the fact that the direct (induced) dipole-dipole interactions between isotropic objects vanish (are averaged out) and only the many-body mutual polarization effects survive the statistical averaging over the external excitation fields.

The pronounced *anisotropy* of the many-body interactions in the cVdW-matter systems also gives rise to a number of phenomena that are qualitatively different from standard VdW-matter, in particular the growth of anisotropic, low-dimensional assemblies - chains, then membranes once a critical size is reached. In a container of finite size, smaller membrane patches are formed, which tend to repel on the average, thus giving rise to dipolar foam structures. The foam exerts a positive pressure onto the walls of the sample container due to the tendency of membranes to increase their surface areas as well as their mutual repulsion. The dipolar foam represents a new and intriguing state of colloidal matter, formed by a delicate interplay of an attractive local interaction and a net repulsive longer range force. Remarkably, both types of forces are born out of a single, conceptually simple cVdW interaction - given by Eq.(14).

The interactions driving the hierarchy of the assembly processes, from dimers to foams are summarized in Figs.10 and 11, where the 2-body and anisotropic 3-body interactions are responsible for the formation of chains, membranes and vesicles, while the membrane-membrane interaction is responsible for the formation of foams in a container with finite volume.

We have also argued that the finite size (finite particle number N) effects in cVdW-matter are very different from other common interactions like VdW or e.g. for classical magnetic beads with permanent moments. The many-body forces are also found to play a crucial role in the *anomalous elastic properties* of chains and membranes. For, instance the bending stiffness of a cVdW ring and the cVdW spherical membrane's stiffness are proportional to $\ln N$ and \sqrt{N} , respectively, which is a direct consequence of the specifically induced long-range many body effects in these systems.

The theory suggests a number of interesting and fea-

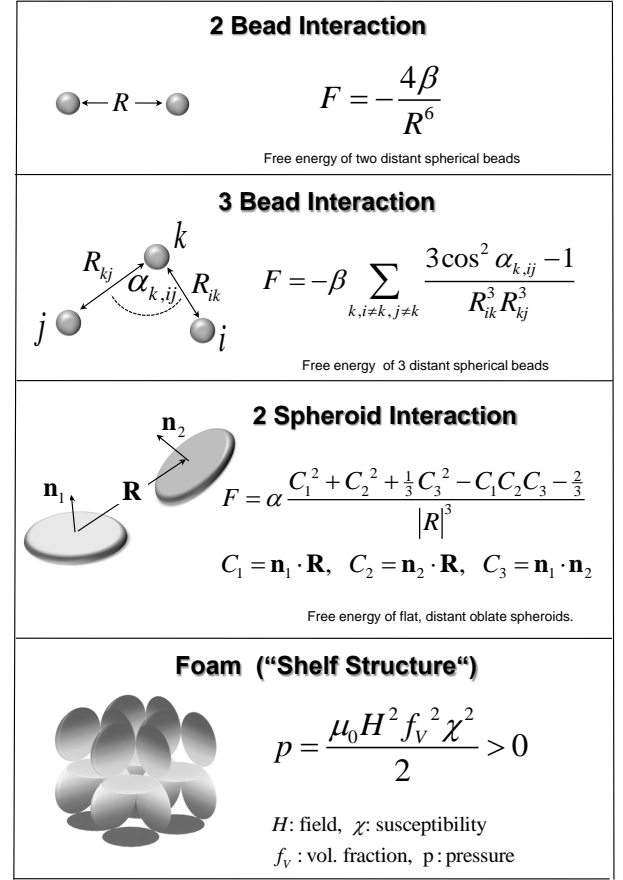


FIG. 10: Summary of main results : Interactions induced by the cVdW interaction.

sible *experiments* that can be performed to test the theoretical predictions about the interactions in the cVdW-matter:

1. It would be very interesting to experimentally probe the dynamics of exactly 3 beads and the behavior of 3-body forces, cf. for instance the surprising attraction/repulsion effects in Fig. 5. The experiment can be performed for microscopic or macroscopic beads (the effect is scale independent). Since 3 beads always span a common plain, the most general dynamics can be observed directly in a single focal plain, e.g. on the microscopy glass-slide on which the beads naturally settle down by gravity.

2. The predicted negative effective surface tension and the instability of millimetric ferrofluid droplets, like in Fig. 6, would be a rather simple experimental test of the theory. Also the shape bistability, i.e. the coexistence of prolate and oblate shapes of the droplets, would be an interesting qualitative outcome to be tested.

3. Bending cVdW chains and flat membrane patches, either by active forces or passively by their own weight and observing their deflections should experimentally reveal the presence of the predicted anomalous, size dependent stiffness.

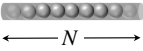
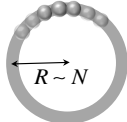
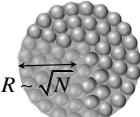
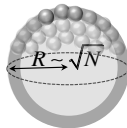
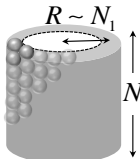
	Linear Chain $F = -c_{ch,1}N + c_{ch,0}$ (Edge Energy = const.)
	Circular Chain $F = -c_{ring,1}N + c_{ring,2} \ln(N)/N$ (Bending Stiffness $\propto \ln R$)
	Flat Disk $F = -c_{mem,1}N + c_{mem,2} \ln(N)\sqrt{N}$ (Line tension $\propto \ln R$)
	Spherical Shell $F = -c_{sph,1}N + c_{sph,2} \sqrt{N}$ (Bending Stiffness $\propto R$)
	Infinite Cylindrical Shell $\frac{F}{N_1 N_2} = -c_{cyl,1} + c_{cyl,2} \frac{1}{N_1}$ (Bending Stiffness $\propto R$)

FIG. 11: Summary of results : Finite size and elastic properties of various structures. The finite size effects (N -effects) in chains, vesicles and membranes are giving rise to anomalous elasticity effects. The free-energies of these respective structures are written in terms of two leading order terms with respect to the particle numbers. The corresponding pre-factors are found in the corresponding sections of the main text.

4. The most telling and fundamental experiment would be to directly probe the equation of state for a foam material. Measuring actively the forces on the container walls or passively observing the rising height of the foam against gravity would be two simple possibilities to test the predicted internal pressure equation for the cVdW foams.

Finally, the central theoretical and experimental question, in our opinion, remains if and how the cVdW can be generally realized in Nature. In particular, we might ask if it can be induced in a truly *equilibrium* system. The previous realizations, in field driven colloidal systems were all non-equilibrium. However there is no principal aspect of the theory that is specific and restricted to a non equilibrium system only. While the driving field amplitudes in our case are externally set, in an equilibrium system they would satisfy a fluctuation dissipation condition which would relate them to the temperature and the

susceptibilities of the particles in the system. We might speculate that in some long-range correlated fluctuating media, like those considered in [26] (see also [27]) the cVdW can indeed be realized even in equilibrium. If the fluctuations of the medium are sufficiently longer ranged than the typical sizes of the formed structures, the assembly will be driven by the cVdW interactions instead of the VdW ones on these scales.

It is important to note that a simple tweak in the way how the interaction is induced (by switching from incoherent to coherent excitation), enormously increases the "morphogenic capacity" of the interaction i.e. its ability to form complex structures. If we are interested in the self-assembly of anything more complex than a spherical droplet (for which the standard VdW-matter is good enough), cVdW-matter would be a better candidate than the simple VdW one. The exploration and utilization of novel non-equilibrium (field-driven) or equilibrium realizations of cVdW interactions is an interesting future challenge. It could open the doors to deeper many-body studies of complex self-assembled materials, and more importantly to technological applications of the potentially very versatile and powerful cVdW-matter.

IX. ACKNOWLEDGEMENTS

We thank Jim Martin, A.Johner, H.Mohrbach, for discussions and comments.

X. APPENDIX 1

A. Calculation of The cVdW Dimer Free-Energy

In the two-particle problem the dipole operator \hat{T} in Eq. (9) has only one non-vanishing component ($\hat{T}_{12} = \hat{T}_{21} \neq 0$) and can be written as:

$$\hat{T} = \varphi_{12} \cdot \begin{pmatrix} 0 & \hat{1} - 3\hat{N} \\ \hat{1} - 3\hat{N} & 0 \end{pmatrix}$$

where $\hat{N} = |\mathbf{b}_{12}\rangle \langle \mathbf{b}_{12}|$ is the projector on the bond vector of the two particles and the scalar factor $\varphi_{12} = V_b/4\pi |\mathbf{R}_{12}|^3$ as introduced before. Using the relations $\hat{N}^2 = \hat{N}$, $(\hat{1} - a\hat{N})^{-1} = \hat{1} + a(1-a)^{-1}\hat{N}$ and the fact that \hat{N} and $\hat{1}$ (or any scalar function like φ_{12}) commute the operator inversion in $\hat{\chi}_{eff} = \chi_b(\hat{1} + \chi_b\hat{T})^{-1}$ is quickly evaluated

$$\hat{\chi}_{eff} = \begin{pmatrix} A_1\hat{1} + A_2\hat{N} & B_1\hat{1} + B_2\hat{N} \\ B_1\hat{1} + B_2\hat{N} & A_1\hat{1} + A_2\hat{N} \end{pmatrix} \quad (75)$$

with the bead distance dependent (scalar) coefficients

$$A_1 = \frac{\chi_b}{1 - \chi_b^2 \varphi_{12}^2}, A_2 = \frac{3\chi_b^3 \varphi_{12}^2}{(1 - \chi_b^2 \varphi_{12}^2)(1 - 4\chi_b^2 \varphi_{12}^2)}$$

$$B_1 = -\frac{\chi_b^2 \varphi_{12}}{1 - \varphi_{12}^2 \chi_b^2}, B_2 = \frac{3\chi_b^2 \varphi_{12} (1 - 2\varphi_{12}^2 \chi_b^2)}{(1 - \varphi_{12}^2 \chi_b^2)(1 - 4\varphi_{12}^2 \chi_b^2)}$$

The relevant quantity for the coherent and the incoherent VdW - the trace of $\hat{\chi}_{eff}$ over the 3 spacial directions- is directly obtained by taking into account that $Tr \hat{N} = 1$ and $Tr \hat{1} = 3$, which gives Eq.(18) in the main text.

XI. APPENDIX 2

A. The Free-Energy for The Three-Body Problem in cVdW Systems

If we consider only 3 beads the interaction energy is given by $\bar{\mathcal{F}}_{cVdW}^{(3)} = -\beta \sum_{k=1,2,3} \sum_{i \neq k, j \neq k} w_{k,ij}$ with $w_{k,ij} = (3 \cos^2 \theta_{k,ij} - 1) / |\mathbf{R}_{ki}|^3 |\mathbf{R}_{kj}|^3$. We put two beads 1 and 2 very close to each other at distance $R_{12} = d$ and the 3-rd one at distance $R_{13} \approx R_{23} \approx R \gg d$. Altogether we have $3 \times 2 \times 2 = 12$ terms in the sum. The terms with flipped $i \rightarrow j$ indices are identical so we can reorder:

$$-\bar{\mathcal{F}}_{cVdW}^{(3)} / \beta = (w_{1,22} + w_{1,33} + 2w_{1,23}) \quad (76)$$

$$+ (w_{2,11} + w_{2,33} + 2w_{2,13})$$

$$+ (w_{3,11} + w_{3,22} + 2w_{3,21})$$

Whenever an index repeats (e.g. as in $w_{3,11}, w_{3,22}$ etc) we have a 2-body force. Then the terms are symmetric and we have $w_{1,22} = w_{2,11}$, $w_{2,33} = w_{3,22}$, $w_{1,33} = w_{3,11}$:

$$-\bar{\mathcal{F}}_{cVdW}^{(3)} / \beta = (2w_{1,22} + 2w_{1,33} + 2w_{2,33}) \quad (77)$$

$$+ (2w_{2,13} + 2w_{1,23} + 2w_{3,21})$$

As $R_{13} \approx R_{23} \approx R$ and $R_{12} = d \ll R$ we have $w_{2,13} \approx w_{1,23}$ (as $\theta_{2,13} \approx \pi - \theta_{1,23}$ and so $\cos^2 \theta_{2,13} = \cos^2 \theta_{1,23}$), one has $w_{1,33} \approx w_{2,33}$ so that

$$-\bar{\mathcal{F}}_{cVdW}^{(3)} / \beta \approx (2w_{1,22} + 4w_{1,33}) + (4w_{1,23} + 2w_{3,21}). \quad (78)$$

Further we have $w_{1,22} \approx \frac{1}{d^6} (3 - 1)$, $w_{1,33} \approx w_{3,21} \approx (3 - 1) / R^6$ and $w_{1,23} \approx (3 \cos^2 \theta_{1,23} - 1) / d^3 R^3$. Keeping only the lowest power in R it simplifies to

$$-\frac{\bar{\mathcal{F}}_{cVdW}^{(3)}}{\beta} = \frac{4}{d^6} + \frac{4(3 \cos^2 \theta_{1,23} - 1)}{d^3 R^3} + O(R^{-6}). \quad (79)$$

B. 3-Body Free-Energy of Finite cVdW Chain

For the finite chain we consider the limit of the chain being still long enough that the two ends do not see each

other (summations for each particle are infinite in one direction). Then we have $3 \cos^2 \theta_{k,ij} - 1 = 2$ and we can split up the summation

$$\bar{\mathcal{F}}_{cVdW, ch}^{(3)} = -\beta \sum_{k=1}^N f_k = -2\beta \sum_{k=1}^{N/2} f_k \quad (80)$$

with

$$f_k = \sum_{j=1, j \neq k}^N \sum_{i=1, i \neq k}^N \frac{2}{|\mathbf{R}_{ik}|^3 |\mathbf{R}_{kj}|^3} \quad (81)$$

$$= 2 \left(\sum_{i=1, i \neq k}^N \frac{1}{|\mathbf{R}_{ik}|^3} \right)^2$$

The upper sum can be subdivided in two parts, one left and one right of the particle k with one of the sums approximated by an infinite boundary $N = \infty$

$$\sum_{i=1, i \neq k}^N \frac{1}{|\mathbf{R}_{ik}|^3} \approx \frac{1}{D^3} \left(\sum_{i=1}^{k-1} \frac{1}{i^3} + \sum_{l=1}^{\infty} \frac{1}{l^3} \right) \quad (82)$$

$$= \frac{2\zeta(3) - S_k}{D^3}$$

with $S_k = \sum_{i=k}^{\infty} (1/i^3)$. Therefore $f_k = 2 \frac{1}{D^6} (2\zeta(3) - S_k)^2$ and the free-energy per particle is given by

$$\frac{\bar{\mathcal{F}}_{cVdW, ch}^{(3)}}{N\beta} \approx -\frac{2}{D^6} \frac{1}{N} \sum_{k=1}^N (2\zeta(3) - S_k)^2. \quad (83)$$

For large k we approximate S_k by integral which gives $S_k \approx 1/2k^2$ and this

$$\frac{\bar{\mathcal{F}}_{cVdW, ch}^{(3)}}{N\beta} \approx -\frac{8\zeta^2(3)}{D^6} + \frac{3.4}{ND^6}. \quad (84)$$

This first term is for the infinite chain, while the second is the leading order correction as expected $O(1/N)$.

C. The 3-Body Free-Energy of Ring in cVdW Systems

Here $\mathbf{R}_{i0} = R(\cos(2\pi i/N), \sin(2\pi i/N))$ (note $\mathbf{R}_{ij} = (R_{x,ij}, R_{y,ij})$, $\cos \theta_{k,ij} = \mathbf{R}_{ik} \cdot \mathbf{R}_{kj} / |\mathbf{R}_{ik}| |\mathbf{R}_{kj}|$). All terms $k = 0, 1, \dots, N-1$ give the same contribution as the term $k = 0$ due to symmetry. We can introduce the angle $\phi_1 = 2\pi i/N$ and $\phi_2 = 2\pi j/N$ with $d\phi \approx 2\pi/N$ (for $N \rightarrow \infty$). Then $\mathbf{R}_{j0} \approx \mathbf{R}(\phi)$

$$|\mathbf{R}(\phi)|^3 = R^3 (2(1 - \cos \phi))^{\frac{3}{2}} \quad (85)$$

$$\cos^2 \theta(\phi_1, \phi_2) = \left(\frac{a_1 a_2 + b_1 b_2}{2\sqrt{a_1 a_2}} \right)$$

where $a_{1,2} = (1 - \cos \phi_{1,2})$ and $b_{1,2} = \sin \phi_{1,2}$. It also holds $\cos^2 \theta(\phi_1, \phi_2) = \cos^2 \left(\frac{\phi_1 - \phi_2}{2} \right)$. With a small distance cutoff angle $c = 2\pi/N$. Then we can write the

free-energy:

$$\begin{aligned} \frac{\bar{\mathcal{F}}_{cVdW,ring}^{(3)}}{\beta N} &= - \sum_{j=1}^{N-1} \sum_{i=1}^{N-1} \frac{3 \cos^2 \theta_{0,ij} - 1}{|\mathbf{R}_{i0}|^3 |\mathbf{R}_{0j}|^3} \quad (86) \\ &= - \frac{1}{2R^6} \sum_{j=1}^{N-1} \sum_{i=1}^{N-1} \frac{1 + 3 \cos(\phi_1 - \phi_2)}{(2a_1)^{\frac{3}{2}} (2a_2)^{\frac{3}{2}}}. \end{aligned}$$

The latter gives most contribution for $\phi_{1/2}$ small and can be expanded around $\phi_{1/2} = 0$. Note that we have 2 identical contributions around $i, j = 1$ and around $N - 1$ in each of the terms. Summing these expanded terms (with $R = \frac{ND}{2\pi}$, $\phi = \frac{2\pi}{N}k$) we arrive at:

$$\frac{\bar{\mathcal{F}}_{cVdW,ring}^{(3)}}{N\beta} \approx - \frac{8\zeta^2(3)}{D^6} + \frac{16\zeta(3)\pi^2 \ln N}{D^6 N^2} \quad (87)$$

D. 3-Body Free-Energy of The cVdW Spherical Shell

For a spherical membrane (coloidosome) with classical elasticity or radius R , we would have an energy density proportional to $1/R^2$ (=curvature²). The total energy coming from the bending (i.e. without self energy of beads) is then $\sim (1/R^2)R^2 \sim 1$ constant. What happens in the case of a coherent coloidosome? Starting again from:

$$\frac{\bar{\mathcal{F}}_{cVdW,sph}^{(3),N}}{\beta} = - \sum'_{i,j,k} \frac{3 \cos^2 \theta_{k,ij} - 1}{|\mathbf{R}_{ik}|^3 |\mathbf{R}_{kj}|^3} \quad (88)$$

with fixed arbitrary $\mathbf{R}_k = R(0, 0, 1)$ (north pole of the sphere, $\mathbf{R} = (R_x, R_y, R_z)$) and $\mathbf{R}_{kj} = R(-\sin \theta_j \cos \phi_j, -\sin \theta_j \sin \phi_j, 1 - \cos \theta_j)$, $|\mathbf{R}_{kj}| = R\sqrt{2(1 - \cos \theta_j)} = 2R \sin(\theta/2)$ and the apex angle is given by $\cos \alpha = \mathbf{R}_{ik} \cdot \mathbf{R}_{kj} / |\mathbf{R}_{ik}| |\mathbf{R}_{kj}|$, where $\alpha \equiv \alpha(\theta_1, \theta_2, \phi_1, \phi_2)$. In order to pick up the N -effects we replace the summation by integration over two spheres where each of the two spheres contains $N = 4\pi R^2 / \rho_{sph}^{-1} \pi (D/2)^2 = 16\rho_{sph} R^2 / D^2$ beads giving the sphere radius: $(\sqrt{N}D/4\rho_{sph}^{1/2}) = R$. The summation can be replaced by double integral over the sphere with surface element $dA_{1,2} = R^2 \sin \theta d\phi d\theta$, and the energy can be written as:

$$\frac{\bar{\mathcal{F}}_{cVdW,sph}^{(3)}}{N \cdot \Gamma} = - \int \left(\frac{3 \cos^2 \alpha - 1}{|\mathbf{R}(\theta_1)|^3 |\mathbf{R}(\theta_2)|^3} \right) dA_1 dA_2 \quad (89)$$

with $\Gamma = \beta N^2 / (4\pi R^2)^2$ and the latter is calculated by an integration (in Mathematica) over ϕ_1 and ϕ_2

$$\frac{\bar{\mathcal{F}}_{cVdW,sph}^{(3)}}{N\beta} = - \frac{\rho_{pack}^2}{8R^2 D^4} \left(\int_{\theta_{\min}(D)}^{\pi} \frac{3 \cos \theta - 1}{\sin^3(\frac{\theta}{2})} \sin \theta d\theta \right)^2 \quad (90)$$

with $\theta_{\min}(D)$ being the angular cut-off resulting from the spherical angle relation (surface area of bead / surface area of whole sphere) : $\Omega(D) = \int_0^{2\pi} \int_0^{\theta_{\min}(D)} \sin \theta d\theta d\phi \approx 2\pi(1/2)\theta_{\min}^2$ but on the other hand $\Omega(D) = \pi(D/2)^2 / 4\pi R^2 = \rho_{sph}/N$ so that $\theta_{\min} = \sqrt{\rho_{sph}/\pi N}$. The integral can be done which gives the energy per particle of the spherical shell:

$$\frac{\bar{\mathcal{F}}_{cVdW,sph}^{(3)}}{N\beta} \approx - \frac{50\pi\rho_{sph}^2}{D^6} \left(1 - \frac{4\sqrt{\rho_{sph}}}{\sqrt{\pi}\sqrt{N}} \right) \quad (91)$$

E. The Microscopic Energy of the cVdW Tubular Membrane

For an infinite cylinder of radius R_{\perp} again we have a high symmetry (all beads are the same) and we can choose the apex point anywhere, say at $(x, y, z) = (1, 0, 0)$. The other points along the cylinder we parameterize cylindrically with coordinates (ϕ, z) , so that the difference vector becomes $\mathbf{R}_{kj} = (R_{\perp}(\cos \phi_j - 1), R_{\perp} \sin \phi_j, z)$ and its length $R_{kj} = \sqrt{z_j^2 + 2R_{\perp}^2(1 - \cos \phi_j)}$. The apex angle is $\cos \alpha_{k,ij} = \mathbf{R}_{ki} \cdot \mathbf{R}_{kj} / R_1 R_2$ with $R_{1/2} = \sqrt{z_{1/2}^2 + 2R_{\perp}^2 a_{1/2}}$.

The energy density consists of seven terms :

$$\frac{\bar{\mathcal{F}}_{cVdW,tub}^{(3)}}{-\beta N} = \sum'_{i,j} \frac{3 \cos^2 \theta_{k,ij} - 1}{|\mathbf{R}_{ik}|^3 |\mathbf{R}_{kj}|^3} \quad (92)$$

$$\begin{aligned} \frac{\bar{\mathcal{F}}_{cVdW,tub}^{(3)}}{-\beta N} &= \frac{3(C_1^2 + C_2^2 + C_3^2 + 2C_4^2)}{R_{\perp}^6} \quad (93) \\ &+ \frac{3(2C_5^2 + 2C_6^2) - C_7^2}{R_{\perp}^6} \end{aligned}$$

Some of the sums are trivially zero due to symmetry: $C_4 = 0$ ($R(\phi, z)$ even but $(\cos \phi - 1) \sin \phi$ odd in ϕ) $C_5 = 0$ (odd in z), $C_6 = 0$ (odd in z and ϕ). Those which are different from zero are

$$C_1 = \sum_{k=\pm 1, \dots, \pm \frac{1}{\delta}} \sum_{l=0, \pm 1, \dots, \pm \infty} \frac{(\cos(\delta k) - 1)^2}{P^5(k, l)} \quad (94)$$

$$C_2 = \sum_{k=\pm 1, \dots, \pm \frac{1}{\delta}} \sum_{l=0, \pm 1, \dots, \pm \infty} \frac{\sin^2(\delta k)}{P^5(k, l)}, \quad (95)$$

$$C_3 = \sum_{k=\pm 1, \dots, \pm \frac{1}{\delta}} \sum_{l=0, \pm 1, \dots, \pm \infty} \frac{(\delta l)^2}{P^5(k, l)} \quad (96)$$

$$C_7 = \sum_{k=\pm 1, \dots, \pm \frac{1}{\delta}} \sum_{l=0, \pm 1, \dots, \pm \infty} \frac{1}{P^3(k, l)} \quad (97)$$

where $P(k, l) = (l^2 \delta^2 + 2(1 - \cos k\delta))^{1/2}$. To obtain the scaling we introduced small scale cutoffs $\delta = D/R_\perp$. Parameterizing the angle $\phi = \delta \cdot k$ with $k = \pm 1, \pm 2, \pm 3, \dots \pm \frac{1}{\delta}$ and the z displacement as $z = \delta \cdot l$ (with $l = 0, \pm 1, \pm 2, \dots \pm \infty$) one can approximate the summation over l by integration. As the final result this gives for $C_1 \approx (2/3\delta^2)$, $(C_2/2) \approx C_3$, $\approx (4\zeta(2)/3\delta^3) \approx C_7$. When inserting $\delta = \frac{D}{R_\perp}$ we get then the final result for the cylinder free-energy ($N = N_1 N_2$, $R_\perp \sim N_1$ - see Fig.11):

$$\frac{\bar{\mathcal{F}}_{cVdW,tub}^{(3)}}{\beta N} \approx -\frac{8\pi^4}{27} \frac{1}{D^6} + \frac{40\pi^2}{27} \frac{1}{R_\perp D^5}. \quad (98)$$

$$\frac{\bar{\mathcal{F}}_{cVdW,sph}^{(3)}}{N\beta} \approx -\frac{50\pi\rho_{sph}^2}{D^6} \left(1 - \frac{4\sqrt{\rho_{sph}}}{\sqrt{\pi}\sqrt{N}}\right) \quad (99)$$

XII. APPENDIX 3

A. Demagnetization Tensors of Spheroids and Cylinders

In calculating magnetic fields of magnetized bodies and the corresponding magnetostatic energy two kind of demagnetization tensors appear [22–24]. The first one is related to the demagnetizing field of the uniformly magnetized body $\mathbf{H}_D(\mathbf{r}) = -\hat{L}(r)\mathbf{M}(\mathbf{r})$ where $\mathbf{M}(\mathbf{r}) = M\mathbf{D}(\mathbf{r})$. Here $\mathbf{M} = \text{const}$ and $D(\mathbf{r})$ is the dimensionless shape function which represents the region of the space bounded by the body (sample) surface, i.e. $D(\mathbf{r}) = 1$ inside the body and $D(\mathbf{r}) = 0$ outside it. Its Fourier transform $D(\mathbf{k})$ - the shape amplitude, which is related to $\hat{L}(r)$ [22–24]

$$\begin{aligned} \hat{L}(\mathbf{r}) &= \frac{1}{(2\pi)^3} \int d^3k \hat{L}(\mathbf{k}) e^{i\mathbf{k} \cdot \mathbf{r}} \\ \hat{L}(\mathbf{k}) &= \frac{D(\mathbf{k})}{k^2} |\mathbf{k}\rangle \langle \mathbf{k}|. \end{aligned} \quad (100)$$

Note, that $(\hat{L}(\mathbf{k}))_{ij} = D(\mathbf{k})k_i k_j / k^2$. The shape amplitude $D(\mathbf{k})$ and $\hat{L}(r)$ are calculated for various bodies. For instance, for sphere of radius R one has $D(\mathbf{k}) = (4\pi R^2/k)j_1(kR)$ where the spherical Bessel function of first order $j_1(x) = (\sin x/x^2) - \cos x/x$. For other body-shapes see more in [22–24] and references therein.

The second type of demagnetization tensor(factors) appears in the expression for the magnetostatic (demagnetization) energy with the uniform magnetization $\mathbf{M}(\mathbf{r}) = \mathbf{M}$

$$\begin{aligned} E_D &= -\frac{\mu_0}{2} \int_{V_D} d^3r \mathbf{M}(\mathbf{r}) \mathbf{H}_D(\mathbf{r}) \\ &= \frac{\mu_0}{2} V_D \mathbf{M} \langle \hat{L}(r) \rangle \mathbf{M}, \end{aligned} \quad (101)$$

where V_D is the volume of the body and $\langle \hat{L}(r) \rangle$ is the *magnetometric* (volume averaged) *demagnetization tensor*, i.e.

$$\begin{aligned} \langle \hat{L}(r) \rangle &= \frac{1}{V_D} \int_{V_D} d^3r \hat{L}(\mathbf{r}) \\ &= \frac{1}{(2\pi)^3 V_D} \int d^3k \frac{D^2(\mathbf{k})}{k^2} |\mathbf{k}\rangle \langle \mathbf{k}| \end{aligned} \quad (102)$$

It is easy to show that the trace of $\hat{L}(\mathbf{r})$ inside the body is one, while outside is zero, i.e. $\text{Tr} \hat{L}(\mathbf{r}) = D(\mathbf{r})$. The magnetometric tensor fulfills $\text{Tr} \langle \hat{L}(r) \rangle = 1$. Note, that in Eq.(40) enter the diagonal components of the magnetometric demagnetization tensor $\langle \hat{L}(r) \rangle$. Since we study magnetic bodies where $\hat{L}(r) = \text{const} = \hat{L}$ inside the body, then $\langle \hat{L}(r) \rangle = \hat{L}$. We give the exact and asymptotic expressions for the L_z demagnetization factor for ellipsoids and cylinders which are important for the studies in the main text.

(i) *Demagnetization factors for ellipsoids* - If a, b, c are the semi-axis of ellipsoid with $\tau_a = (c/a)$, $\tau_b = (c/b)$, $k = \arcsin \sqrt{1 - \tau_a^{-2}}$, $m = (1 - \tau_b^{-2})/(1 - \tau_a^{-2})$ than one has [22–24]

$$L_z(\tau_a, \tau_b) = \frac{1}{\tau_a \tau_b} \frac{F(k, m) - E(k, m)}{m \sin^3 k}, \quad (103)$$

where $E(k, m)$ and $F(k, m)$ are incomplete elliptic integrals [28]. The symmetry implies $L_x(\tau_a, \tau_b) = L_z(\tau_a^{-1}, \tau_b \tau_a^{-1})$ and $L_y(\tau_a, \tau_b) = L_z(\tau_a \tau_b^{-1}, \tau_b^{-1})$ - see [22–24]. For oblate and prolate spheroids, where $\tau_a = \tau_b = \tau_s$, one has

$$L_z(\tau_s) = \frac{1}{1 - \tau_s^2} \left[1 - \frac{\tau_s \arccos(\tau_s)}{\sqrt{1 - \tau_s^2}} \right] \quad (104)$$

For $\tau_e \rightarrow 0$ (extreme oblate, i.e. membrane-like spheroid) it gives

$$L_z(\tau_s) = 1 - \frac{\pi}{2} \tau_s + 2\tau_s^2 + O(\tau_s^3), \quad (105)$$

and for $\tau_e \rightarrow \infty$ (extreme prolate, i.e. chain-like spheroid) one has

$$L_z(\tau_s) = \frac{\ln(2\tau_s/e)}{\tau_s^2} + O(\tau_s^{-4}). \quad (106)$$

(ii) *Demagnetization factors for cylinders* - For cylinders with thickness (height) t and radius R with the aspect ratio $\tau = t/2R$ and $\kappa = 1/\sqrt{1 + \tau^2}$ one has [22–24]

$$L_z^{cyl}(\tau) = 1 + \frac{4}{3\pi\tau} \left\{ 1 - \frac{1}{\kappa} [(1 - \tau^2)E(\kappa^2) + \tau^2 K(\kappa^2)] \right\} \quad (107)$$

where $E(\kappa^2)$ and $K(\kappa^2)$ are complete elliptic functions [28].

For *very thin cylinder* where $\tau \rightarrow 0$ one has

$$L_z^{cyl}(\tau) = 1 + \frac{\tau}{\pi} \left(1 + 2 \ln \frac{\tau}{4} \right) + O(\tau^3). \quad (108)$$

For *very long cylinder* where $\tau \rightarrow \infty$ one has

$$L_z^{cyl}(\tau) = \frac{4}{3\pi\tau} - \frac{8}{\tau^2} + O(\tau^{-4}). \quad (109)$$

B. Surface and Demagnetization Factors For Deformed Sphere

The aspect ratio of the spheroid is $\tau_s = c/a$. Close to the sphere one has $\varepsilon = \tau_s - 1 \ll 1$, where $\varepsilon < 0$ is for oblate ellipsoid while $\varepsilon > 0$ is for the prolate one. By using Eq.(104) one has for small $|\varepsilon| \ll 1$ one has

$$L_z^{prol/obl} = \frac{1}{3} - \frac{4}{15}\varepsilon + \frac{6}{35}\varepsilon^2 - \frac{32}{315}\varepsilon^3 + \frac{40}{693}\varepsilon^4 + O(\varepsilon^5) \quad (110)$$

Similarly for the surface of the prolate spheroid one has

$$A_{prolate} = 2\pi a^2 \left(1 + \frac{\tau_s}{x} \sin^{-1} x \right), \quad (111)$$

with $x^2 = 1 - 1/\tau_s^2$ for $\tau_s > 1$ and for the oblate one

$$A_{oblate} = 2\pi a^2 \left(1 + \frac{1-x^2}{x} \tanh^{-1} x \right), \quad (112)$$

for $x^2 = 1 - \tau_s^2$ for $\tau_s < 1$. In the following analysis the volume is fixed, i.e. $V = 4\pi a^2 c/3 = 4\pi a^3 \tau_s/3$, $a^2 = (3V/4\pi\tau_s)^{2/3}$ and in terms of the axial stretching one has

$$\frac{A_{prolate}}{A_0} = \frac{1 + \frac{(\varepsilon+1)^2}{\sqrt{\varepsilon(\varepsilon+2)}} \arcsin \sqrt{1 - \frac{1}{(\varepsilon+1)^2}}}{2(\varepsilon+1)^{2/3}} \quad (113)$$

for $\tau_s > 1$ and

$$\frac{A_{oblate}}{A_0} = \frac{1 + \frac{(\varepsilon+1)^2}{\sqrt{-\varepsilon(\varepsilon+2)}} \operatorname{arctanh} \sqrt{-\varepsilon(\varepsilon+2)}}{2(\varepsilon+1)^{2/3}} \quad (114)$$

for $\tau_s < 1$, with $A_0 = 4\pi(3V/4\pi)^{2/3}$ the initial area of the sphere. We can expand the surface area $A_{prol/obl}(\varepsilon)$ (expansions coincide):

$$\frac{A_{prol/obl}(\varepsilon)}{A_0} = 1 + \frac{8}{45}\varepsilon^2 - \frac{584}{2835}\varepsilon^3 + \frac{118}{567}\varepsilon^4 + O(\varepsilon^5) \quad (115)$$

XIII. APPENDIX 4

A. Membrane-Bead Interaction in cVdW Systems

In order to calculate the free-energy in Eq.(59) we need to know $Tr\hat{\chi}_{m,eff}$ and $Tr\hat{\chi}_{b,eff}$ where

$$\hat{\chi}_{m,eff} = (1 - q_m q_b \varphi_0^2 \hat{\chi}_m \hat{t} \hat{\chi}_b \hat{t})^{-1} \hat{\chi}_m (1 - q_m \varphi_0 \hat{t} \hat{\chi}_b), \quad (116)$$

with $\hat{t}_{m-b} \equiv \hat{t}$ and $\hat{\chi}_{b,eff}$ is obtained by replacing $m \leftrightarrow b$. For the assumed symmetry and geometry of the problem we have $|\mathbf{n}_m\rangle = \langle \mathbf{b}|$. Here, $q_{m,b} = V_{m,b}/V_0$, $V_0 = V_m + V_b$, and $\hat{\chi}_{m,b}$ is the membrane and bead susceptibility (with respect to external field), respectively, $\varphi_0 = V_0/4\pi R_{mb}^3$. By defining $\hat{N} = |\mathbf{n}_m\rangle \langle \mathbf{n}_m|$ and $\hat{P} = 1 - \hat{N}$ we have $\hat{N}^2 = \hat{N}$, $\hat{P}^2 = \hat{P}$, $\hat{N}\hat{P} = 0$, $Tr\hat{N} = 1$ and $Tr\hat{P} = 2$ and

$$\hat{t} = -2\hat{N} + \hat{P}. \quad (117)$$

Further we parameterize $\hat{\chi}_m = \chi_{\max} \hat{\chi}_m^0$, $\hat{\chi}_m^0 = p_m \hat{N} + \hat{P}$, $p_m = \chi_{\min}/\chi_{\max}$, $\hat{\chi}_b = \chi_b \hat{1}$, $b = \alpha_b \alpha_m$, $\alpha_m = q_m \chi_{\max} \varphi_0$, $\alpha_b = q_b \chi_b \varphi_0$. In this parametrization we have

$$\begin{aligned} \hat{\chi}_{m,eff} &= \chi_{\max} \hat{A}^{-1} \hat{\chi}_m^0 (1 - \alpha_b \hat{t}) \\ \hat{\chi}_{b,eff} &= \chi_b \hat{A}^{-1} (1 - \alpha_m \hat{\chi}_m^0 \hat{t}) \end{aligned} \quad (118)$$

and

$$\hat{A} = 1 - b \chi_m^0 \hat{t}^2. \quad (119)$$

By using the projecting properties of \hat{N} and \hat{P} one obtains the inverse matrix \hat{A}^{-1}

$$\hat{A}^{-1} = \frac{1}{1-b} \left[1 - \frac{c}{1+c} \hat{N} \right] \quad (120)$$

with $c = b(1 - 4p_m)/(1 - b)$. After some algebra one obtains the effective membrane susceptibility

$$\hat{\chi}_{m,eff} = \frac{\chi_{\max}}{1-b} \left\{ a \hat{1} + \left[\frac{p_m(1+2\alpha_b)}{1+c} - a \right] \hat{N} \right\} \quad (121)$$

where $a = (1 - \alpha_b)$. Then the trace is

$$Tr\hat{\chi}_{m,eff} = \frac{\chi_{\max}}{1-b} \left\{ 2(1 - \alpha_b) + \frac{p_m(1+2\alpha_b)}{1+c} \right\}. \quad (122)$$

Analogously one obtains the effective bead susceptibility $Tr\hat{\chi}_{b,eff}$

$$Tr\hat{\chi}_{b,eff} = \frac{\chi_b}{1-b} \left\{ \frac{3+2c}{1+c} + 2\alpha_m \left(\frac{p_m}{1+c} - 1 \right) \right\}. \quad (123)$$

By inserting Eq.(122) and Eq.(123) into Eq.(59) one obtains w_m and w_b in Eq.(62) and Eq.(63), respectively.

B. Derivation of the 2-Membrane Interaction in cVdW Systems

Having in mind two identical membranes (with volume V_m) we consider susceptibilities $\hat{\chi}_1$ and $\hat{\chi}_2$ of two oblate spheroids, which are differently oriented in space. In terms of their own local coordinate systems (in Dirac bra-ket notation for tensors) they are given by

$$\begin{aligned}\hat{\chi}_1 &= \chi_{\min} |\mathbf{n}_1\rangle \langle \mathbf{n}_1| + \chi_{\max} (\hat{1} - |\mathbf{n}_1\rangle \langle \mathbf{n}_1|) \\ \hat{\chi}_2 &= \chi_{\min} |\mathbf{n}_2\rangle \langle \mathbf{n}_2| + \chi_{\max} (\hat{1} - |\mathbf{n}_2\rangle \langle \mathbf{n}_2|),\end{aligned}\quad (124)$$

where the unit vectors $|\mathbf{n}_1\rangle$, $|\mathbf{n}_2\rangle$ are the normals of the membranes 1 and 2 respectively. By using Eq.(124), and noting that $Tr\{\hat{\chi}_1\hat{\chi}_2\} = Tr\{\hat{\chi}_2\hat{\chi}_1\}$, $Tr\{\hat{\chi}_1\hat{\chi}_2(|\mathbf{b}_{21}\rangle \langle \mathbf{b}_{21}|)\} = Tr\{\hat{\chi}_2\hat{\chi}_1(|\mathbf{b}_{12}\rangle \langle \mathbf{b}_{12}|)\}$ and $Tr\{|\mathbf{n}_i\rangle \langle \mathbf{n}_j|\} = \langle \mathbf{n}_i | \mathbf{n}_j \rangle$ (with $\mathbf{a} \cdot \mathbf{b} \equiv \langle \mathbf{a} | \mathbf{b} \rangle$ the scalar product) it follows

$$Tr\{\hat{\chi}_1\hat{\chi}_2\} = \chi_{\max}^2 [1 + 2\gamma + c_3^2(1 - \gamma)^2] \quad (125)$$

$$\begin{aligned}\frac{Tr\{\hat{\chi}_1\hat{\chi}_2(|\mathbf{b}_{12}\rangle \langle \mathbf{b}_{12}|)\}}{\chi_{\max}^2} &= [1 - (1 - \gamma)(c_1^2 + c_2^2) \\ &\quad + (1 - \gamma)^2 c_1 c_2 c_3],\end{aligned}\quad (126)$$

where $\gamma = (\chi_{\min}/\chi_{\max})$ and $c_1 = \mathbf{n}_1 \cdot \mathbf{b}_{12}$, $c_2 = \mathbf{n}_2 \cdot \mathbf{b}_{12}$, $c_3 = \mathbf{n}_1 \cdot \mathbf{n}_2$ are factors describing the mutual orientation of membranes. By replacing Eqs.(125-126) in Eq.(58) (where V_b in φ_{12} is replaced by the membrane volume V_m) one obtains Eq.(65) in the manuscript.

C. The Interaction Energy of The Cubic Shelf Structure

The lattice sum $S(\equiv a_M^3 \bar{\mathcal{F}}_{int}/\alpha)$, $\alpha = 9\eta\chi_{\max}^2\mu_0 H_0^2 V_m^2/16\pi$ (where $\mathbf{r}_{i1} = \mathbf{R}_{i1}/a_M$ and $\eta = (1 - \chi_{\min}/\chi_{\max})/3$) for the cubic shelf structure is given by

$$S = \sum_{1,\kappa=x,y,z} \frac{\eta C_{3,\kappa}^2 + C_{1,\kappa}^2 + C_{2,\kappa}^2 - 3\eta C_{1,\kappa} C_{2,\kappa} C_{3,\kappa} - \frac{2}{3}}{r_{1,\kappa}^3}, \quad (127)$$

where for compactness we define $C_{1/2/3,\kappa} = C_{1/2/3,1,\kappa}$. The coefficients $C_1 = \mathbf{n}_1 \cdot \mathbf{b}_{12}$, $C_2 = \mathbf{n}_2 \cdot \mathbf{b}_{12}$, $C_3 = \mathbf{n}_1 \cdot \mathbf{n}_2$ where \mathbf{n}_1 and \mathbf{n}_2 are normals to membrane 1 and 2, respectively, while \mathbf{b}_{12} is the unit bonding vector. The summation over unit cells labeled by $l = (l_x, l_y, l_z)$ comprises interactions of membrane at the point $\mathbf{r}_{1,\kappa} = (0, 0, 0)$ and with the normal to the membrane plane parallel to the z-axis, i.e. $\mathbf{n}_z^0 = (0, 0, 1)$, with all others. The summation over $\kappa = x, y, z$ means the interaction with membranes whose normals \mathbf{n}_x , \mathbf{n}_y , \mathbf{n}_z are along the x , y , z -axis, respectively. For further calculations we parameterize $\mathbf{n}_1 = (0, 0, 1)$, $\mathbf{n}_2 = \cos\phi_2 \sin\theta_2, \sin\phi_2 \sin\theta_2, \cos\theta_2$ and for \mathbf{b} the same as for \mathbf{n}_2 but ϕ_2, θ_2 goes to ϕ_b, θ_b . It is straightforward to show that $C_{3,\kappa=x} = C_{3,\kappa=y} = 0$. Similarly, $C_{3,\kappa=z} = 1$, $C_{1,\kappa=z} = l_z/\sqrt{l_x^2 + l_y^2 + l_z^2}$ and that $C_{1,\kappa=z} = C_{2,\kappa=z}$. It turns out that $C_{1,\kappa=x} = (l_z - 1/2)/\sqrt{(l_x - 1/2)^2 + l_y^2 + (l_z - 1/2)^2}$, and analogously for $C_{2,\kappa=x}$, $C_{1,\kappa=y}$, $C_{2,\kappa=y}$. Based on these results the sum in Eq.(127) has the final form

$$\begin{aligned}S &= 2 \sum_{l_x, l_y} \sum_{l_z=1}^{\infty} \frac{A(l_x, l_y, l_z)}{(l_x^2 + l_y^2 + l_z^2)^{3/2}} \\ &\quad + 2 \sum_{l_x, l_y} \sum_{l_z=-\infty}^{\infty} \frac{B(l_x, l_y, l_z)}{(l_x^2 + (l_y - \frac{1}{2})^2 + (l_z - \frac{1}{2})^2)^{3/2}}\end{aligned}\quad (128)$$

where

$$A(l_x, l_y, l_z) = \alpha + \frac{l_z^2}{l_x^2 + l_y^2 + l_z^2} - \frac{2}{3}$$

$$B(l_x, l_y, l_z) = \frac{(l_y - \frac{1}{2})^2 + (l_z - \frac{1}{2})^2}{l_x^2 + (l_y - \frac{1}{2})^2 + (l_z - \frac{1}{2})^2} - \frac{2}{3}$$

$\alpha = (1 - \chi_{\min}/\chi_{\max})/3$ and the sum over l_x, l_y goes from $-\infty$ to ∞ .

-
- [1] V. I. Balykin, V. G. Minogin and V. S. Letokhov, Rep. Prog. Phys. 63, 1429 (2000).
 - [2] W.B.Russel, D.A.Saville, and W.R. Schowalter, Colloidal Dispersions, Cambridge, Cambridge University Press (1989)
 - [3] Berry, M V, Proc.Roy.Soc.Lond. A 452, 1207, (1996)
 - [4] I. W. Hamley, The Physics of Block Copolymers, Oxford Science Publications, (1999)
 - [5] A. Tsebers, M. Maiorov. Magnetohydrodynamics, vol. 16, 21–27 (1980); Rosensweig R E, Zahn M and Shu-

- movich R J. Magn. Magn. Mater. 39, 127-32 (1983)
- [6] D. G. Ravenhall, C. J. Pethick, and J. R. Wilson, Phys. Rev.Lett. 50, 2066 (1983); M. Hashimoto, H. Seki, and M. Yamada, Prog. Theor. Phys. 71, 320 (1984).
- [7] I. M. Kulić and M. L. Kulić, Phys. Rev.Lett. 111, 198301 (2013).
- [8] J. E. Martin, R. A. Anderson, R. L. Williamson, J. Chem. Phys. 118, 1557 (2003)
- [9] J. E. Martin, E. Venturini, G. L. Gulley, J. Williamson, Phys. Rev. E 69, 021508-1 (2004)

- [10] N. Osterman, I. Poberaj, J. Donikar, D. Frenkel, P. Ziherl, D. Babić, Phys. Rev. Lett. **103**, 228301 (2009)
- [11] J. F. Douglas, Nature 463, 302 (2010)
- [12] In the previous paper [7] we called it *spatially coherent fluctuation interaction* but find that the former name (cVdW) is physically more elucidating.
- [13] V.A. Parsegian, Van Der Waals Forces, Cambridge University Press (2006); D. Langbein, Theory of Van der Waals Attraction, Springer Tracts in Modern Physics, Vol.(72), Springer-Verlag, Berlin, 1974
- [14] W. A. Bullough, Proceedings of the 5th. International Conference on Electrorheological Fluids, Magneto-rheological Suspensions and Associated Technology, Singapore: University of Scheffield, Scheffield. World Scientific, 1996; M. Nakano, K. Koyama, Proceedings of the 6th. International Conference on Electrorheological Fluids, Magneto-rheological Suspensions and Associated Technology, Singapore: Southern Illinois University, Carbondale. World Scientific, 1998; R. Tao, Proceedings of the 7th. International Conference on Electrorheological Fluids, Magneto-rheological Suspensions and Associated Technology, Singapore: Yamagata University, Japan. World Scientific, 2000..
- [15] L. D. Landau, E. M. Lifshitz, Electrodynamics of Continuous Media, Oxford: Pergamon Press (1989)
- [16] T. B. Jones, Electromechanics of Particles, Cambridge Universities Press, 1995
- [17] We adopt the magnetic notation but all results apply in the electric formalism (paramagnets become dielectrics)
- [18] B. M. Axilrod, E. Teller, J. Chem. Phys. **11**, 299 (1943); Yu. S. Barash, V. L. Ginzburg, Sov. Phys. Uspekhi, **143**, 345 (1984)
- [19] The χ^2 scaling is valid for equilibrium conditions, where a detailed ballance between the moments and (thermal or quantum) bath hold. The scaling for icFI switches to $\propto \chi^3$ if the fluctuating field is exogeneous (externally set) and non-equilibrium as in the present cVdW case.
- [20] Note, when $i \neq j$ the Eq.(26) contains both 2-body interactions as well as the non-local 3-body ones (for instance 12, 23, etc.) - see discussion below. Similarly Eq.(27) contains besides the 3-body interactions also the non-local 4-body ones (for instance 12, 23, 34, etc), which property is contained also in all higher order terms.
- [21] D. R. Nelson, Defects and Geometry in Condensed Matter Physics, Cambridge University Press, 2002
- [22] M. Beleggia, M. De Graef, Y. T. Millev, J. Phys. D: Appl. Phys. **39**, 891 (2006); M. Beleggia, M. De Graef, Y. T. Millev, D. A. Goode, G. Rowlands, J. Phys. D: Appl. Phys. **38**, 3333 (2005)
- [23] M. Beleggia, M. De Graef, J. of Mag. and Mag. Mat., **263**, L1-L9 (2003); M. Beleggia, S. Tandon, Y. Zhu, M. De Graef, J. of Mag. and Mag. Mat., **278**, 270 (2004)
- [24] S. Tandon, M. Beleggia, Y. Zhu, M. De Graef, J. of Mag. and Mag. Mat., **271**, 9 (2004); S. Tandon, M. Beleggia, Y. Zhu, M. De Graef, J. of Mag. and Mag. Mat., **271**, 27 (2004)
- [25] J. E. Martin, private communication
- [26] H. Li and M. Kardar, Phys. Rev. A 46, 6490 (1992)
- [27] M. Kardar and R. Golestanian, Rev. Mod. Phys., 71, 1233 (1999)
- [28] M. Abramowitz, I. Stegun, Handbook of Mathematical Functions, New York: Dover (1972)